AD-A148 387 A THEORETICAL VIEW ON THE STRESS ANALYSIS OF FULLY INFLATED PARACHUTE CANOPIES(U) NAVAL SURFACE WEAPONS CENTER SILVER SPRING MD W P LUDTKE 28 MAY 84 1/1

UNCLASSIFIED NSWC/TR-84-204 F/G 1/3 NL

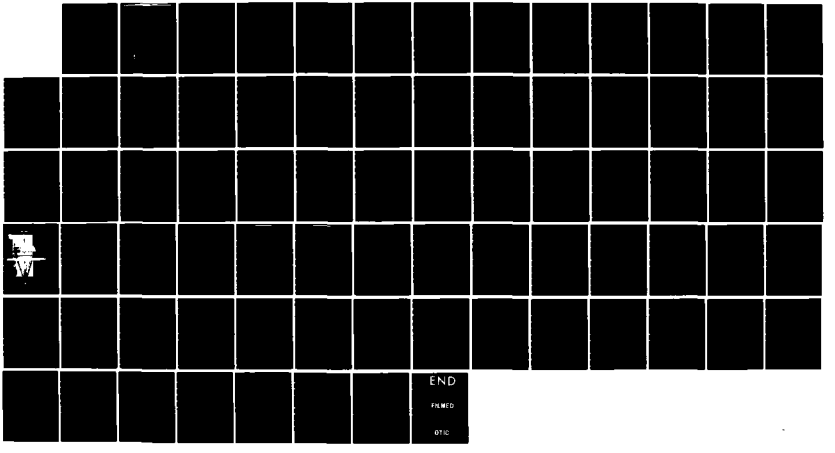

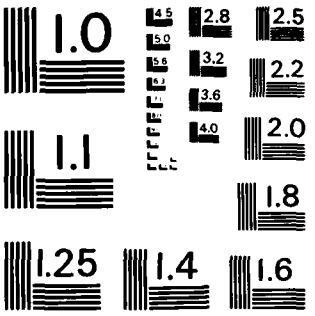

MICROCOPY RESOLUTION TEST CHART
NATIONAL BUREAU OF STANDARDS-1963-A

(12)

NSWC TR 84-204

A THEORETICAL VIEW ON THE STRESS ANALYSIS OF FULLY INFLATED PARACHUTE CANOPIES

BY W. P. LUDTKE

UNDERWATER SYSTEMS DEPARTMENT

28 MAY 1984

Approved for public release; distribution unlimited.

NAVAL SURFACE WEAPONS CENTER

Dahlgren, Virginia 22448 • Silver Spring, Maryland 20910

UNCLASSIFIED

SECURITY CLASSIFICATION OF THIS PAGE (When Data Entered)

REPORT DOCUMENTATION PAGE	READ INSTRUCTIONS BEFORE COMPLETING FORM
1. REPORT NUMBER NSWC TR 84-204	2. GOVT ACCESSION NO. AD A148387
3. RECIPIENT'S CATALOG NUMBER	
4. TITLE (and Subtitle) A THEORETICAL VIEW ON THE STRESS ANALYSIS OF FULLY INFLATED PARACHUTE CANOPIES	5. TYPE OF REPORT & PERIOD COVERED
	6. PERFORMING ORG. REPORT NUMBER
7. AUTHOR(s) W. P. Ludtke	8. CONTRACT OR GRANT NUMBER(s)
9. PERFORMING ORGANIZATION NAME AND ADDRESS Naval Surface Weapons Center (U13) White Oak Silver Spring, Maryland 20910	10. PROGRAM ELEMENT, PROJECT, TASK AREA & WORK UNIT NUMBERS O&M, N 4U15MA
11. CONTROLLING OFFICE NAME AND ADDRESS	12. REPORT DATE 28 May 1984
	13. NUMBER OF PAGES 75
14. MONITORING AGENCY NAME & ADDRESS(if different from Controlling Office)	15. SECURITY CLASS. (of this report) UNCLASSIFIED
	15a. DECLASSIFICATION/DOWNGRADING SCHEDULE

16. DISTRIBUTION STATEMENT (of this Report)

Approved for public release; distribution unlimited.

17. DISTRIBUTION STATEMENT (of the abstract entered in Block 20, if different from Report)

18. SUPPLEMENTARY NOTES

19. KEY WORDS (Continue on reverse side if necessary and identify by block number)

Parachute
Cloth stress
Canopy shape
Force distribution
Stress analysis
Pressure distribution

20. ABSTRACT (Continue on reverse side if necessary and identify by block number)

This report describes a theoretical approach to the analysis of the force distribution in fully inflated parachute canopies based upon the inflated gore mainseam shape. Normal and tangential forces for any arbitrary point along the gore mainseam can be determined and the magnitude and location of the maximum normal force and cloth stress evaluated. Methods, criteria, and rationale for calculating the force distributions are presented.

DD FORM 1 JAN 73 1473 EDITION OF 1 NOV 65 IS OBSOLETE

S/N 0102-LF-014-6601

UNCLASSIFIED

SECURITY CLASSIFICATION OF THIS PAGE (When Data Entered)

FOREWORD

This report describes a theoretical approach to the analysis of the force distribution in fully inflated parachute canopies based upon the inflated gore mainseam shape. Normal and tangential forces for any arbitrary point along the gore mainseam can be determined and the magnitude and location of the maximum normal force and cloth stress evaluated. Methods, criteria, and rationale for calculating the force distributions are presented.

Approved by:

GEORGE KALAF, Head
Mine Warfare Division

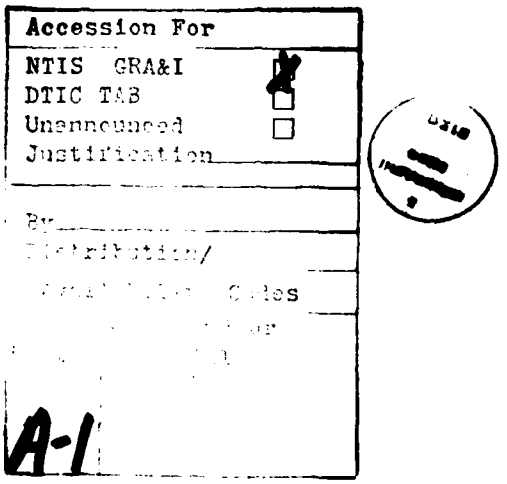

CONTENTS

	Page
INTRODUCTION	1
CANOPY STEADY STATE INFLATED SHAPE	1
LOAD-LINE CONCEPT	2
NORMAL FORCE DISTRIBUTION ALONG THE LOAD LINE	2
LOADING PER UNIT ARC LENGTH	7
COMPARISON OF THE NORMAL FORCE DISTRIBUTION ALONG THE LOAD LINE AND THE DRAG FORCE PER SUSPENSION LINE	11
DETERMINATION OF THE FORCE TANGENT TO THE BILLOWED CLOTH AT THE LOAD LINE	15
MINIMUM TANGENTIAL FORCE	17
TANGENTIAL FORCE IN THE CANOPY CLOTH AT AN ARBITRARY POINT ON THE LOAD LINE	24
FORCE RESOLUTION IN THE CANOPY CLOTH OF SOLID CLOTH PARACHUTES	31
FORCE RESOLUTION IN THE CANOPY CLOTH OF RINGSLOT PARACHUTES	33
COMMENTS ON WIND TUNNEL TESTING	36
EXAMPLE 1: STRESS ANALYSIS OF A 24-GORE RINGSLOT PARACHUTE OF 24-FOOT D_o DIAMETER	36
CANOPY PRESSURE DISTRIBUTION	48
THE FULLY INFLATED STATE	48
REFERENCES	59
DEFINITIONS	61
NOMENCLATURE	63

ILLUSTRATIONS

Figure		Page
1	PARACHUTE STEADY STATE INFLATED SHAPE	3
2	VISUALIZATION OF THE LOAD-LINE CONCEPT	5
3	FORCE DIAGRAM AT AN ARBITRARY POINT ALONG THE LOAD LINE	6
4	SIMPLIFIED FORCE SYSTEM	7
5	INFLATED PARACHUTE PROFILE SHAPES FOR EQUAL DRAG AREA CROSS TYPE CANOPY VERSUS A 16-GORE 24-PERCENT GEOMETRICALLY POROUS RIBBON CANOPY	8
6	COORDINATE SYSTEM FOR ELLIPTICAL ARC LENGTH	9
7	CANOPY LOAD LINE NORMAL FORCE DISTRIBUTIONS AS FUNCTIONS OF dß FOR 16-GORE 24-PERCENT GEOMETRICALLY POROUS RIBBON PARACHUTE	12
7A	CANOPY LOAD-LINE NORMAL-FORCE DISTRIBUTIONS AS FUNCTIONS OF dß FOR 16 SUSPENSION LINE CROSS PARACHUTE	13
8	DIAGRAM FOR NORMAL FORCE SUMMATION	14
9	BILLOWED GORE GEOMETRY FOR AN ARBITRARY POINT ON THE LOAD LINE	18
10	BILLOWED GORE GEOMETRY FOR MINIMUM STRESS	20
11	COMPARISON OF CONVENTIONAL FLAT CIRCULAR PARACHUTE GORE LAYOUT AND MINIMUM CLOTH STRESS GORE CONFIGURATION	21
12	EFFECT OF EXCESS CLOTH BILLOW ON RADIUS OF CURVATURE	22
13	VARIATION OF MINIMUM CLOTH STRESS GORE GEOMETRY AS A FUNCTION OF GORE LENGTH	23
14	GORE BILLOW FOR 2θ = 180 DEGREES	26
15	TRANSCENDENTAL EQUATION θ/SIN θ SOLUTION AS A FUNCTION OF θ	28
16	SHAPE OF AN INFLATED GORE REPRODUCED FROM REF (4)	29
17	EFFECT OF ANGLE ϕ ON THE CLOTH TANGENTIAL FORCE STRESS	30
18	FORCE RESOLUTION IN THE CANOPY CLOTH	32
19	WIND TUNNEL TEST PHOTOGRAPH OF THE 24-GORE 16-PERCENT GEOMETRICALLY POROUS PARACHUTE OF TABLE 2	34
20	HEM FORCES IN A RINGSLOT PARACHUTE CIRCUMFERENTIAL RIBBON	35
21	CIRCUMFERENTIAL RIBBON HEM RAKE ANGLES VERSUS PERCENT OF GORE LENGTH	35
22	UNBILLOWED GORE GEOMETRY FOR THE RINGSLOT PARACHUTE OF EXAMPLE 1	41
23	BILLOWED GORE GEOMETRY FOR THE RINGSLOT PARACHUTE OF EXAMPLE 1	46
24	NORMAL FORCE PER UNIT OF GORE LENGTH VERSUS PERCENT OF GORE LENGTH FOR THE RINGSLOT PARACHUTE OF EXAMPLE 1	49
25	EFFECT OF GORE BILLOW ON THE GORE BILLOW ANGLE FOR THE RINGSLOT PARACHUTE OF EXAMPLE 1	50
26	EFFECT OF GORE BILLOW ON THE CANOPY CLOTH RADIUS OF CURVATURE FOR THE RINGSLOT PARACHUTE OF EXAMPLE 1	51

ILLUSTRATIONS (Cont.)

Figure		Page
27	CANOPY CLOTH TANGENTIAL FORCE PER UNIT LENGTH VERSUS PERCENT OF GORE LENGTH FOR THE RINGSLOT PARACHUTE OF EXAMPLE 1	52
28	EFFECT OF GORE BILLOW ON THE ANGLE ϕ AND STRESS CONCENTRATION FACTOR FOR THE RINGSLOT PARACHUTE OF EXAMPLE 1	53
29	ESTIMATED STATIC PRESSURE DISTRIBUTIONS ALONG THE GORE LENGTH FOR BILLOWED AND UNBILLOWED GORES FOR THE RINGSLOT PARACHUTE OF EXAMPLE 1	57

TABLES

Table		Page
1	SUMMARY OF PARACHUTE SHAPE TEST RESULTS FOR 12-GORE AND 16-GORE CONFIGURATIONS	4
2	SUMMARY OF PARACHUTE SHAPE TEST RESULTS FOR 24-GORE AND 30-GORE CONFIGURATIONS	4
3	NUMERICAL INTEGRATION OF AXIAL FORCE	16
4	BILLOW CONFIGURATIONS AND EFFECTS	25
5	EFFECT OF THE NUMBER OF GORES ON THE CANOPY CLOTH FORCE LEVELS OF SOLID CLOTH PARACHUTES	31
6	STRESS ANALYSIS SUMMARY OF THE 24-FOOT, 24-GORE RINGSLOT PARACHUTE OF EXAMPLE 1	37
7	TENSILE FORCES IN THE HEM OF THE CIRCUMFERENTIAL RINGS AND TEARING FORCES AT THE GORE MAINSEAM OF THE RINGSLOT PARACHUTE OF EXAMPLE 1	39
8	ACCURACY OF ARC LENGTH CALCULATIONS FOR VARIOUS VALUES OF $d\beta/2$	43
9	RANGE OF AVERAGE STEADY STATE CANOPY PRESSURE COEFFICIENTS	56
10	EFFECT OF GORE BILLOW ON THE CANOPY PRESSURE DISTRIBUTION	58

INTRODUCTION

The complexity of analyzing the force distribution in a parachute is as much a psychological problem as it is technical. Faced with the many angles, surfaces, radii of curvature, and three dimensional awesomeness of the inflated parachute structure, the engineer can at first feel overwhelmed. With this in mind, I have attempted to devise a simple method of analysis. The technique is derived from the "law of strings" and is based upon the premise that the parachute inflated shape is developed from the interaction of the canopy-gore shape, the suspension-line length, and the applied aerodynamic forces.

The forces in the canopy cloth are transmitted through the gore mainseams and suspension lines to the attached payload. The inflated shape of the mainseam-suspension line system is caused by a distribution of forces which are normal to the mainseam at all points along the arc from the canopy hem to the vent. While the normal force distribution along the canopy mainseam-suspension line system cannot be directly measured, we can record the effects of the normal force distribution; i.e., the inflated mainseam-suspension line system shape. Once the geometry of the inflated mainseam shape has been determined theoretically the rest of the parachute canopy may be temporarily discarded and the normal force distribution required along the mainseam in order to yield the particular inflated shape calculated.

A coordinate system related to the tangent angle between the gore mainseam and the parachute center line is used to calculate the magnitude of the canopy normal force, tangent force, and the coordinates of application. At this point the parachute canopy is reintroduced into the analysis, and the force distributions in the canopy surface calculated at any arbitrary point, maximum loads determined, and the variation of canopy geometry on forces assessed.

Methods for analysis of the canopy geometry and force distributions are presented, and a method of estimating a static canopy pressure distribution is suggested.

CANOPY STEADY STATE INFLATED SHAPE

One analysis requirement is that the coordinates of the inflated mainseam and the slope of the tangent to the coordinates be known. This can be accomplished from photographs by the use of descriptive geometry or by the methods of References 1, 2, or 3. Reference 1 presents methods for determining inflated gore coordinates and angles. References 2 and 3 demonstrated that the steady state inflated gore mainseam shapes of several parachute types consist of

two elliptical sections of common major diameter, $2\bar{a}$, and different minor diameters b and b'. The generalized inflated gore mainseam is illustrated in Figure 1, and scale factors for determining the inflated shape are reproduced from References 2 and 3 in Tables 1 and 2. The canopy shapes of References 2 and 3 are to be used in the analysis as they permit the expression of the inflated shape as $y = f(x)$ and the slope angle $\beta = f'(x)$, but the analysis is not limited by this.

LOAD-LINE CONCEPT

The aerodynamic drag force exerted by the parachute is a predictable and measurable quantity. The equilibrium between the applied aerodynamic forces, the geometry of the canopy gores, the suspension-line length and confluence point define a particular parachute's characteristic steady state inflated shape and transient shape during the inflation process. Therefore, it seems reasonable to assume that if applied distributed forces determine a parachute's inflated shape that the converse should be possible. That is, when the shape of the gore mainseam is known the force distribution which produces this shape can be analytically determined.

The "load-line" concept is proposed as an aid to visualizing the problem. The gore mainseam-suspension line assembly is theoretically replaced by a single "load line" having the identical inflated shape and anchored at points A and B of Figure 2. Theoretically the parachute canopy may now be temporarily discarded. Upon determination of the normal forces and load distribution, the forces into the canopy cloth from the load line can be calculated at any arbitrary point, maximum forces determined, and the variation of canopy geometry on forces assessed.

NORMAL FORCE DISTRIBUTION ALONG THE LOAD LINE

The X-Y coordinate system is illustrated in Figure 1. Relative to this coordinate system the inflated canopy shape is defined by equations (1) and (2). It should be noted in all calculations that for values of X greater than zero the minor axis b' must be utilized, and for values of X less than zero the minor axis (b) must be utilized.

$$\frac{X^2}{b^2} + \frac{Y^2}{\bar{a}^2} = 1 \tag{1}$$

$$\tan \beta = - \left(\frac{\bar{a}}{b}\right)^2 \frac{X}{Y} \tag{2}$$

The parameter of variation in the analysis is the tangent angle β. The angle β varies between defined limits from β_0 at the canopy hem to the vent angle β_v, which is determined by the type of parachute, i.e., flat, conical, etc. For a flat type of parachute, the load line is perpendicular to the parachute center line at the vent, i.e., the X axis of the system.

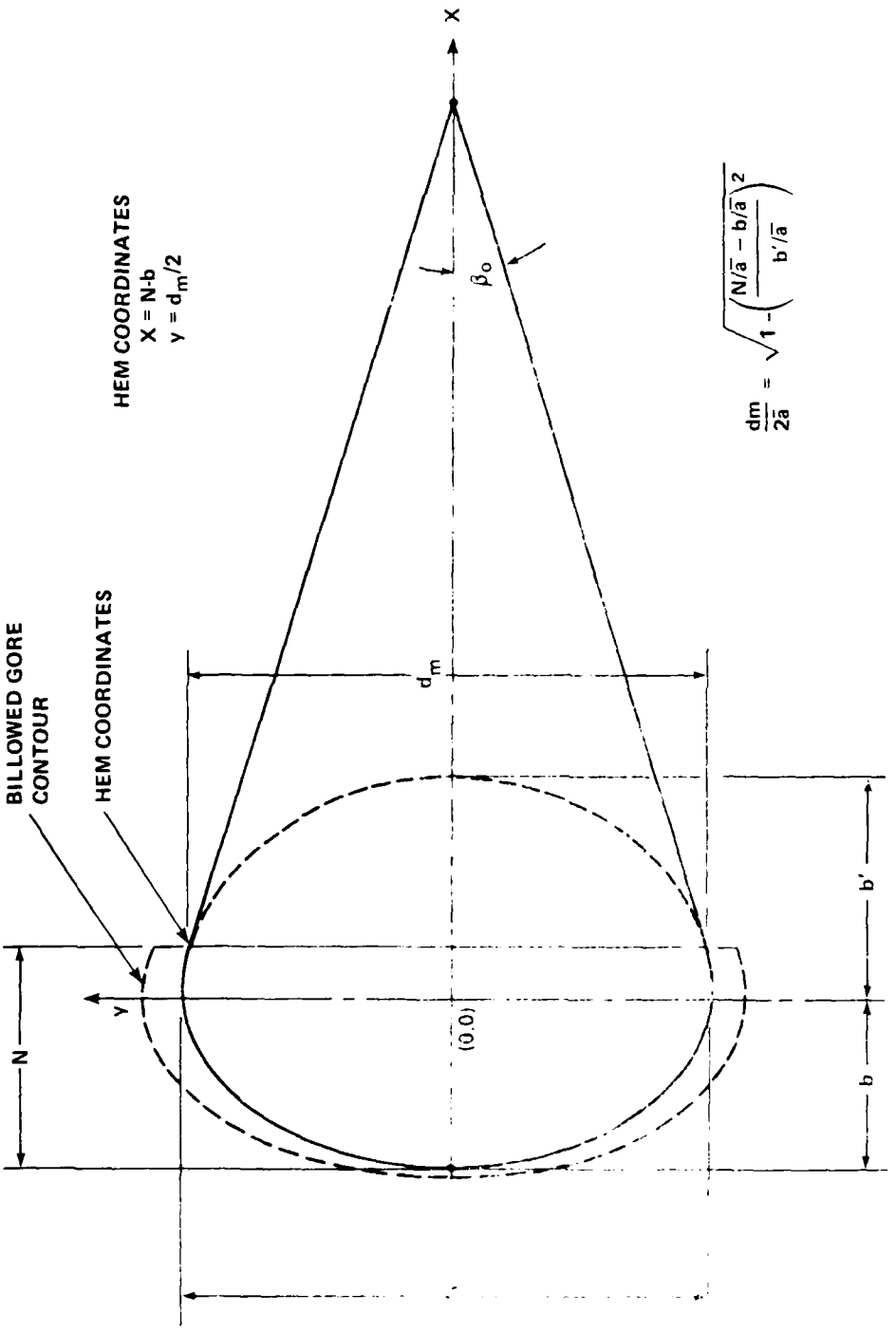

FIGURE1. PARACHUTE STEADY STATE INFLATED SHAPE

TABLE I. SUMMARY OF PARACHUTE SHAPE TEST RESULTS FOR 12-GORE AND 16-GORE CONFIGURATIONS

Parachute Type	No. of Gores	Suspension Line Length inches	Velocity mph	Velocity fps	Scale Factor, K $\frac{2\bar{s}}{D_o}$	$\frac{2\bar{s}}{D_f}$	$\frac{2\bar{s}}{D_R}$	$\frac{2\bar{s}}{L}$	$\frac{N}{a}$	Axes Ratio $\frac{b}{a}$	$\frac{b'}{a}$	$\frac{b}{a} + \frac{b'}{a}$
Flat Circular	12	34	60	73	.645	.650			.856	.6115	.8817	1.4932
	16	34	60	73	.663	.669			.820	.5558	.9039	1.4597
10% Extended Skirt	12	34	100	147	.663	.652			.881	.6424	.8860	1.5284
	16	34	17	25	.654	.640			.785	.5580	.8502	1.4082
Elliptical	12	34	75	110			.916		.812	.5626	.9657	1.5283
	16	34	17	25			.875		.800	.6169	.8163	1.4332
Hemispherical	12	34	125	183			.996		1.254	1.0005	.9080	1.9085
	16	34	75	110			.994		1.185	.9129	.9380	1.8509
Ringslot	12	34	25	37	.607	.654			.853	.6566	.8735	1.530
18% Geometric	12	34	100	147	.616	.663			.922	.6566	.8735	1.530
Porosity	12	34	200	293	.637	.686			.918	.6566	.8735	1.530
	16	34	25	37	.611	.658			.827	.6004	.8890	1.4894
	16	34	100	147	.617	.664			.864	.6004	.8890	1.4894
	16	34	200	293	.645	.695			.844	.6004	.8890	1.4894
Ribbon	12	34	25	37	.586	.832			.859	.6558	.8768	1.5326
24% Geometric	12	34	100	147	.615	.863			.837	.6558	.8768	1.5326
Porosity	12	34	200	293	.632	.881			.877	.6558	.8768	1.5326
	16	34	25	37	.603	.650			.797	.5570	.8578	1.4148
	16	34	100	147	.626	.674			.791	.5570	.8578	1.4148
	16	34	200	293	.648	.698			.781	.5570	.8578	1.4148
Cross Chute W/L = .264		34	25	37	.710			.543	1.242	.8867	1.2776	2.1643
		34	100	147	.707			.540	1.270	.8867	1.2776	2.1643
		34	200	293	.718			.547	1.285	.8867	1.2776	2.1643
		47	25	37	.769			.580	1.113	.8494	1.2512	2.1006
		47	100	147	.729			.557	1.205	.8494	1.2512	2.1006
		47	200	293	.775			.592	1.110	.8494	1.2512	2.1006

REPRODUCED FROM REFERENCE 2

TABLE 2. SUMMARY OF PARACHUTE SHAPE TEST RESULTS FOR 24-GORE AND 30-GORE CONFIGURATIONS

Parachute Type	No. of Gores	Suspension Line Length inches	Velocity mph	Velocity fps	Scale Factor, K $\frac{2\bar{s}}{D_o}$	$\frac{2\bar{s}}{D_f}$	$\frac{N}{a}$	Axes Ratio $\frac{b}{a}$	$\frac{b'}{a}$	$\frac{b}{a} + \frac{b'}{a}$
Flat Circular	24	34	50	73	.677	.679	.795	.5758	.8126	1.3884
	30	34	17	25	.668	.669	.827	.6214	.7806	1.4020
10% Extended* Skirt	24	34	100	147	.665	.648	.834	.5949	.8771	1.4720
	30	34	17	25	.650	.633	.825	.6255	.7962	1.4127
Ring Slot 18% Geometrically Porous	24	34	25	37	.663	.665	.824	.5800	.9053	1.4853
	24	34	100	147	.680	.682	.819	.5800	.9053	1.4853
	24	34	200	293	.694	.696	.809	.5800	.9053	1.4853
	30	34	25	37	.677	.678	.788	.5800	.9053	1.4853
	30	34	100	147	.684	.685	.802	.5800	.9053	1.4853
	30	34	200	293	.698	.699	.800	.5800	.9053	1.4853
Ribbon 24% Geometrically Porous	24	34	25	37	.671	.673	.770	.5980	.8187	1.4167
	24	34	100	147	.676	.678	.813	.5980	.8187	1.4167
	24	34	200	293	.687	.689	.804	.5980	.8187	1.4167
	30	34	25	37	.656	.657	.782	.6021	.8463	1.4484
	30	34	100	147	.669	.670	.784	.6021	.8463	1.4484
	30	34	200	293	.677	.679	.823	.6021	.8463	1.4484

*Since this parachute was "breathing" during the test, several photographs were taken at each speed. The data were reduced from the photograph which most reasonably appeared to represent the equilibrium state.

REPRODUCED FROM REFERENCE 3

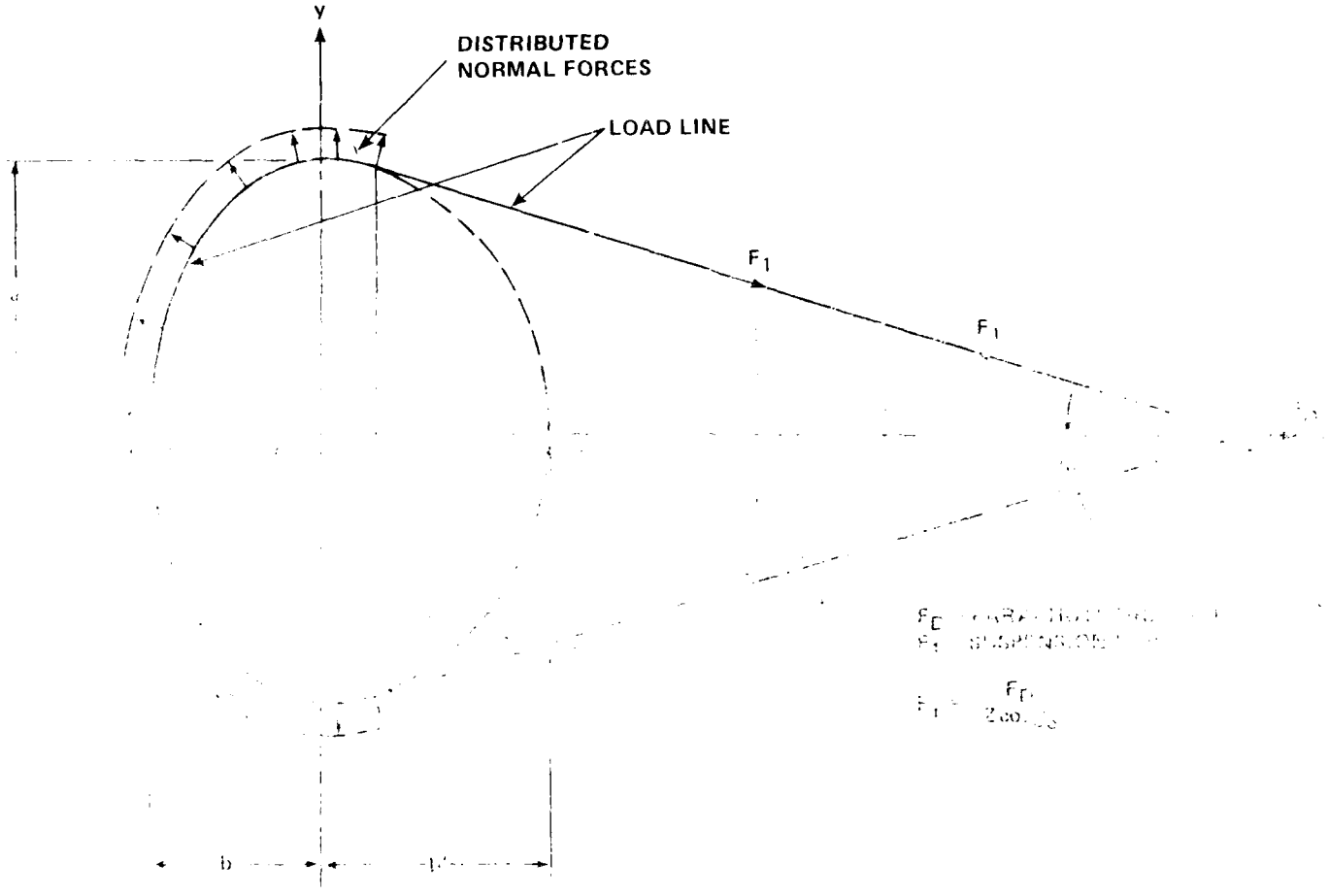

FIGURE 2. VISUALIZATION OF THE LOAD-LINE CONCEPT

The presence of a force normal to the load line results in a change in direction of the load line and the force tangent to the load line. The force diagram for a small change in ß is illustrated in Figure 3 between two arbitrary points, (x_1, y_1) and (x_2, y_2).

As dß approaches zero the summation of the normal forces over the arc length, dℓ, approaches ΣF_N and is assumed to be applied at the coordinate (X_N, Y_N). The coordinate (X_N, Y_N) is located between the two arbitrary

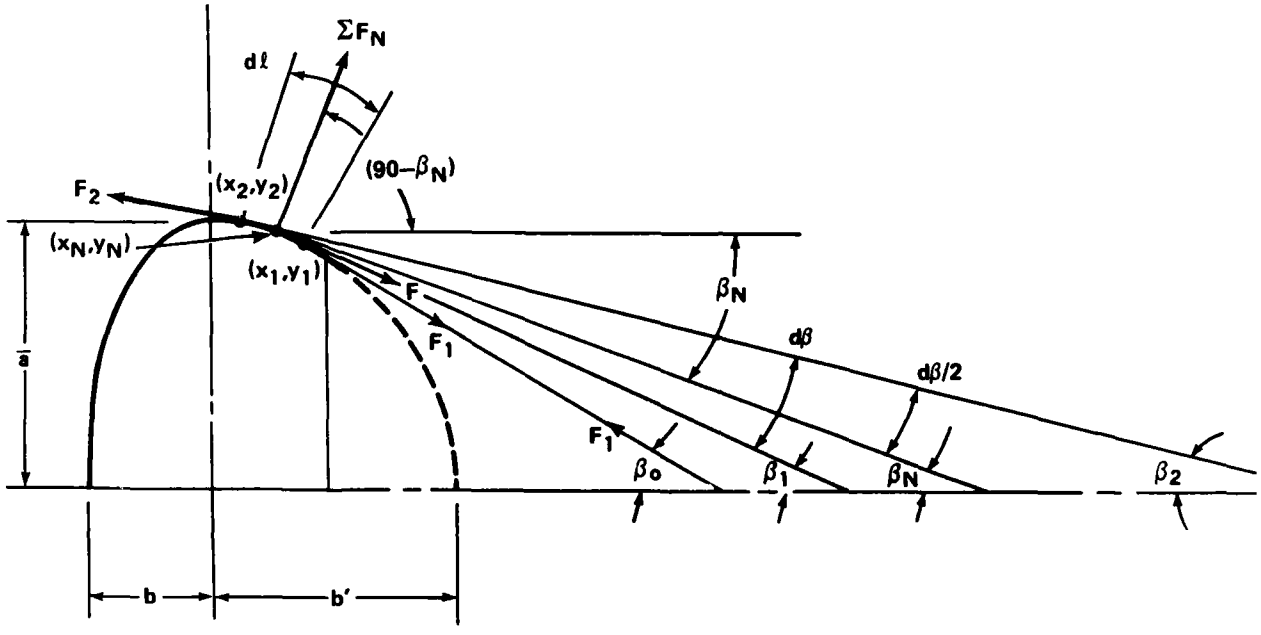

FIGURE 3. FORCE DIAGRAM AT AN ARBITRARY POINT ALONG THE LOAD LINE

points and makes equal angles dß/2 with the tangential force of each coordinate point. The construction of the normal at equal deflection angles is equivalent to assuming a constant tension along the load line. This seems reasonable as dß approaches zero. A simplified force system is shown in Figure 4.

The important conclusion of Equation 4 is that the normal force distribution as a percentage of the suspension-line load F_1 is dependent only upon the angular change dß. For a constant dß along the load line the normal force distribution, $\Sigma F_N/F_1$, is constant and is the same for all types of parachutes. The load line loading in pounds per unit of arc length varies along the load line as the subtended arc length varies for a constant angular dß. The highest unit loading occurs in the region of the maximum inflated diameter where dℓ/dß is a minimum. The theoretical discontinuity of the normal force distribution at the maximum diameter is caused by the substitution of b for b' in the elliptic inflated shape (Equation 1).

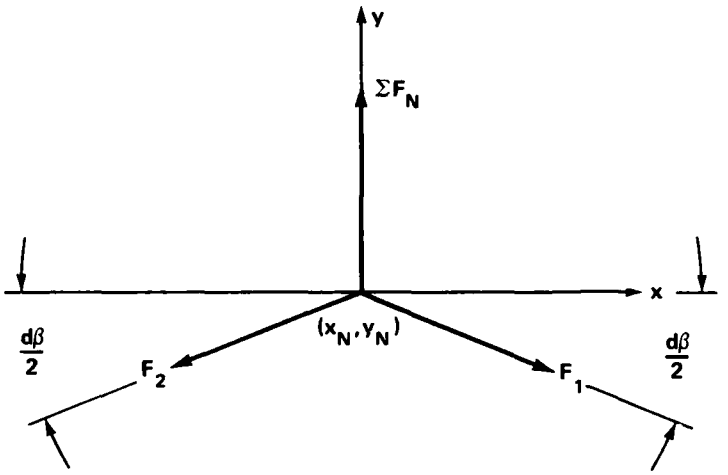

$$\Sigma F_x = F_1 \cos\frac{d\beta}{2} - F_2 \cos\frac{d\beta}{2} = 0 \quad (3)$$

$$F_1 = F_2$$

$$F_1 = \frac{F_D}{Z \cos\beta_0} \quad (3a)$$

$$\Sigma F_y = \Sigma F_N - 2F_1 \sin\frac{d\beta}{2} = 0$$

$$\frac{\Sigma F_N}{F_1} = 2 \sin\frac{d\beta}{2} \quad (4)$$

FIGURE 4. SIMPLIFIED FORCE SYSTEM

LOADING PER UNIT ARC LENGTH

The variation in the inflated load-line shape and suspension-line confluence angle among the several types of parachutes accounts for different loadings per unit length even though the normal force distribution is the same. Figure 5 compares the inflated shapes of the 16-gore Ribbon Parachute and the W/L = 0.264, 16 suspension line Cross Type Parachute of Reference 2 for equal drag areas. For a given dynamic pressure, the following conclusions may be drawn:

a. The steady state drag forces, F_D, of the Cross and Ribbon Parachutes are equal.

b. The suspension-line loads, F_l, are slightly different due to the variation in β_o.

c. The ratio of normal force to suspension-line load, $\Sigma F_N/F_l$, is identical for both canopies for a constant dß as shown by Equation (4). In order to calculate the unit arc length loading in pounds per inch, it is necessary to calculate the arc length between the chosen limits. It is not necessary to calculate the entire arc length to determine local loading. Only the local arc length, $d\ell$, over the angular change dß need be considered. Two methods are available. One method of accomplishing this is to express the x and y coordinates as a function of ß as ß varies from β_o at the skirt hem to the β_v at the vent. The elliptic shape (Equations (1) and (2)) is restated to present the x and y coordinates as functions of ß, the appropriate minor diameter, and the semi-major diameter.

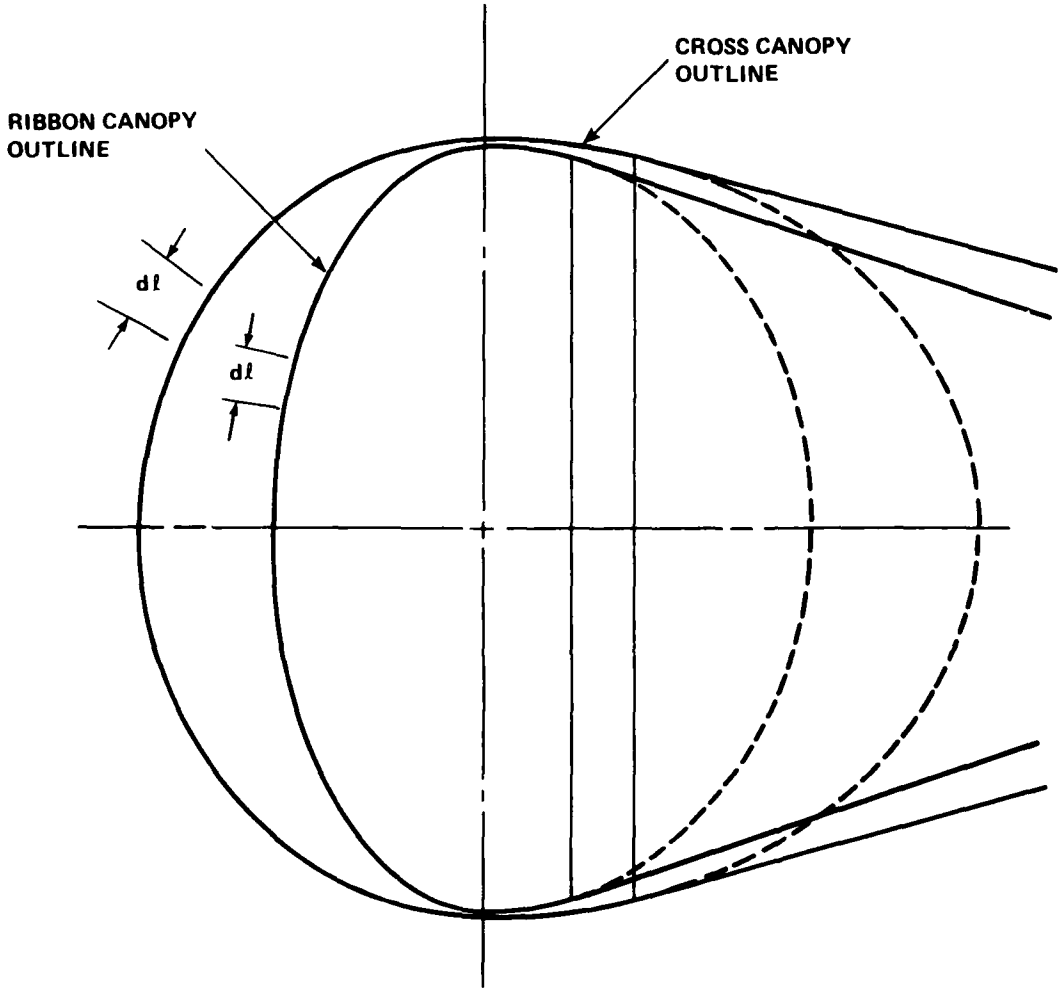

	PARACHUTE	
	RIBBON	CROSS
D_o, ft	16.0	
L, ft		19.3
S_o, ft^2	201.06	170.7
C_D	0.5	0.589
$C_D S_o$, ft^2	100.53	100.53
2a, ft	10.37	10.56
b, ft	2.89	4.68
b', ft	4.45	6.74
N, ft	4.05	6.78
L_s/D_o	1.0	
L_s/L		1.0
β_o, Deg	17.5	14.4

PROFILE SHAPE DATA TAKEN FROM TABLE I FOR 200 MPH TEST VELOCITY, L_s = 34 INCHES

FIGURE 5. INFLATED PARACHUTE PROFILE SHAPES FOR EQUAL DRAG AREA CROSS TYPE CANOPY VERSUS A 16-GORE, 24-PERCENT GEOMETRICALLY POROUS RIBBON CANOPY

$$X = \frac{-b}{\sqrt{1 + \frac{1}{\tan^2 \beta}\left(\frac{\bar{a}}{-b}\right)^2}} \tag{5}$$

$$Y = \pm \bar{a}\sqrt{1 - \left(\frac{x}{-b}\right)^2} \tag{6}$$

and

$$(X_1, Y_1) = f(\beta_1)$$

$$(X_2, Y_2) = g(\beta_1 - d\beta)$$

$$(X_N, Y_N) = h(\beta_1 - \frac{d\beta}{2})$$

With reference to Figure 6, the elliptic arc length between β_1 and β_2 can be determined as follows.

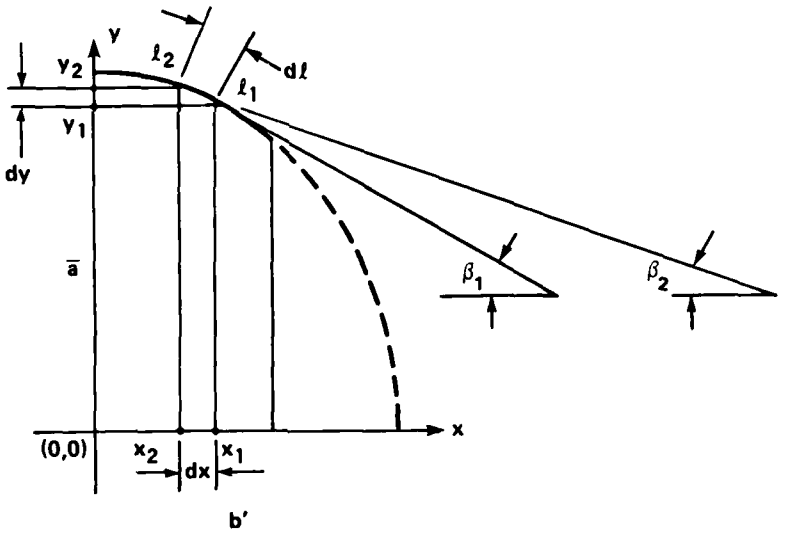

FIGURE 6. COORDINATE SYSTEM FOR ELLIPTICAL ARC LENGTH

$$\int_{\ell_1}^{\ell_2} d\ell = \int_{X_1}^{X_2} \sqrt{1 + \left(\frac{dY}{dX}\right)^2}\, dx$$

from Equation (2)

$$\frac{dY}{dX} = -\left(\frac{\bar{a}}{b'}\right)^2 \frac{X}{Y}$$

$$\left(\frac{dY}{dX}\right)^2 = \left(\frac{\bar{a}}{b'}\right)^4 \left(\frac{X}{Y}\right)^2$$

from Equation (1)

$$\frac{1}{Y^2} = \left(\frac{b'}{\bar{a}}\right)^2 \frac{1}{b'^2 - X^2}$$

therefore

$$\left(\frac{dY}{dX}\right)^2 = \left(\frac{\bar{a}}{b'}\right)^2 \frac{X^2}{b'^2 - X^2}$$

and

$$\int_{\ell_1}^{\ell_2} d\ell = \int_{X_1}^{X_2} \sqrt{1 + \left(\frac{\bar{a}}{b'}\right)^2 \frac{X^2}{b'^2 - X^2}}\, dx \qquad (7)$$

where x_1 and x_2 are determined from Equation (5). Equation (7) can be used to calculate the total arc length from the canopy hem to the maximum diameter and from the maximum diameter to the vent by using appropriate b or b'.

Total arc lengths calculated by Equation (7) have varied from measured arc lengths as much as 6 percent. Some of the reasons for this are:

a. Canopy shape may not be truly described by y = f(x).

b. Effects of elongation due to F_1, may not be fully accounted for.

c. Errors in measurement may exist when taking canopy shapes from relatively small photographs.

The effects of the above conditions can be minimized when translating inflated mainseam measurements to drawing layout coordinates by using percentages of mainseam length. For example, the gore width at 40 percent of the mainseam length should be the same as the drawing layout even though the measured mainseam is in error by a small amount.

The second method can be used to estimate short arc lengths with a desk calculator. The appropriate limits of x_1 and x_2 are again determined from Equation (5) and the y coordinates from Equation (1) then

$$d\ell = \sum_{X_1}^{X_2} \sqrt{(X_2-X_1)^2 + (Y_2-Y_1)^2} \tag{8}$$

The arc length can be calculated to any desired accuracy by successive iterations of Equation (8) and subdividing the constant arc length $d\ell$ to smaller Δx and Δy. This was the method used to calculate the load-line loading per inch of arc length $\Sigma F_N/F_1 d\ell$, in Figures 7 and 7A. Angles β_N were selected at 1°, 10°, 20° ... 80° and 90° and arc lengths calculated over the β range of $\beta_N \pm 1$ degree.

Comparison of the Cross and Ribbon Parachute loadings illustrates that the elliptic nature of the Ribbon Parachute causes a wider variation in loading per inch of arc length than the more nearly hemispherical Cross Parachute for the same load line normal force loading, $\Sigma F_N/F_1$. The maximum normal forces occur at the maximum inflated diameter for both parachutes. A truly hemispherical canopy would have constant normal force and unit loading over the canopy. The minimum unit load line forces occur in the parachute vent area. However, in Figures 16 and 17, the maximum canopy cloth stresses are shown to likely occur in the vent area.

COMPARISON OF THE NORMAL FORCE DISTRIBUTION ALONG THE LOAD LINE AND THE DRAG FORCE PER SUSPENSION LINE

If the developed normal force distribution is a realistic analysis, the parachute drag force per suspension line, F_D/Z, must be equivalent to the summation of the axial components, ΣF_A, of the normal forces at each β_N. Figure 8 illustrates the force diagram used for the normal force summation.

$$F_A = \Sigma F_N \text{Cos}(90°-\beta_N) \tag{9}$$

$$F_A = \sum_{\beta_i}^{\beta_F} [\, F_N \text{Cos}(90°-\beta_N)\,] = \frac{F_D}{Z} \tag{9a}$$

$$\frac{F_D}{Z} = F_1 \, \text{Cos}\beta_o \tag{9b}$$

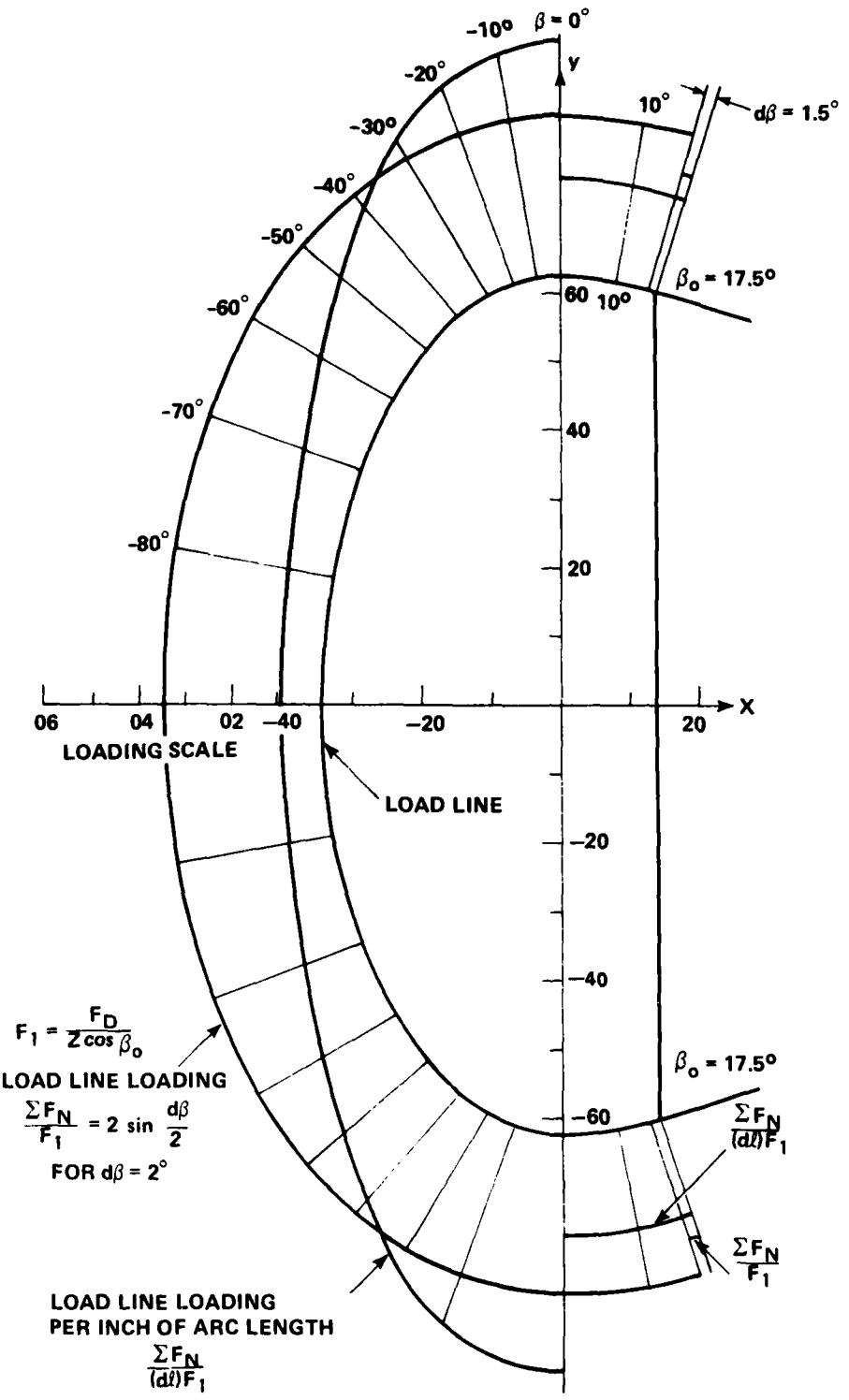

FIGURE 7. CANOPY LOAD LINE NORMAL FORCE DISTRIBUTIONS AS FUNCTIONS OF dβ FOR THE 16-GORE, 24-PERCENT GEOMETRICALLY POROUS RIBBON PARACHUTE

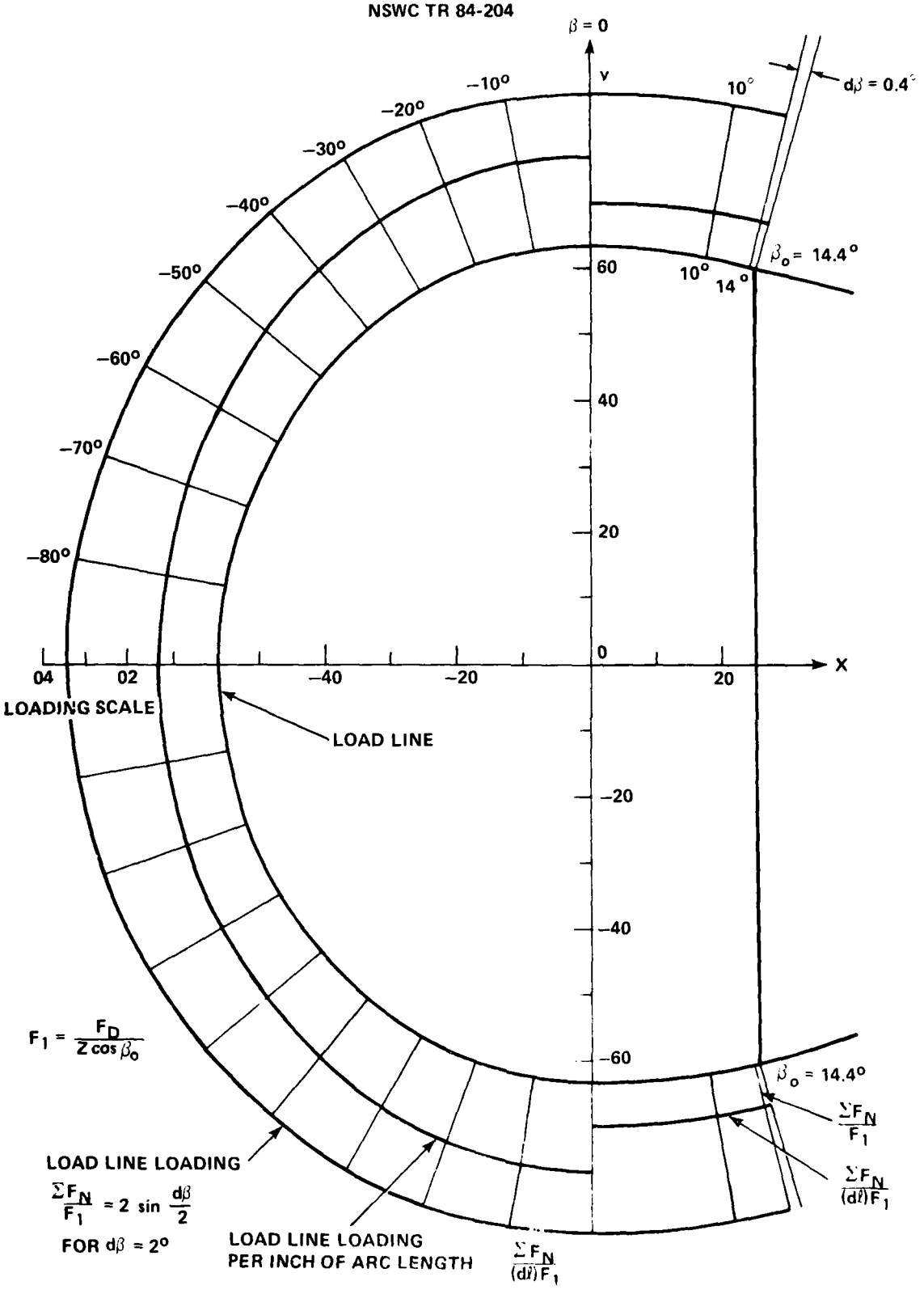

FIGURE 7A. CANOPY LOAD-LINE NORMAL-FORCE DISTRIBUTIONS AS FUNCTIONS OF $d\beta$ FOR THE 16 SUSPENSION LINE CROSS PARACHUTE

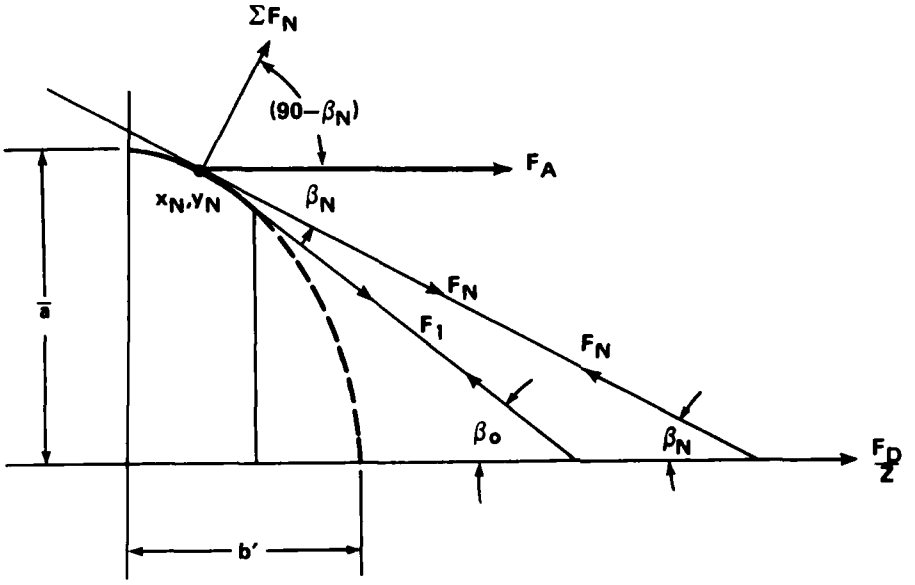

FIGURE 8. DIAGRAM FOR NORMAL FORCE SUMMATION

$$F_N = 2F_1 \sin \frac{d\beta}{2} \tag{3}$$

Therefore,

$$\Sigma F_A = \sum_{\beta_i}^{\beta_F} [2F_1 \sin \frac{d\beta}{2} \cos(90-\beta_N)] = F_1 \cos \beta_0 \tag{9c}$$

$$\Sigma F_A = \sum_{\beta_i}^{\beta_F} [2 \sin \frac{d\beta}{2} \cos(90-\beta_N)] = \cos\beta_0 \tag{9d}$$

As an example let $\beta_o = 18°$, and $d\beta = 2°$.

Then the first $\beta_N = \beta_i$

$$\beta_i = \beta_N = \beta_0 - \frac{d\beta}{2}$$

$$\beta_i = 18° - 1° = 17°$$

and the final $\beta_N = \beta_F$

$$\beta_F = -(\beta_v - \frac{d\beta}{2})$$

$$\beta_F = -(90° - 1°)$$

$$\beta_F = -89°$$

$$\Sigma F_A = \sum_{17°}^{-89°} [2 \sin \frac{d\beta}{2} \cos(90-\beta_N)] = \cos\beta_0$$

$$0.0349 \sum_{17°}^{-89°} \cos(90-\beta_N) = \cos\beta_0$$

The summation of the Cos $(90 - \beta_N)$ for each β_N from 17 to -89 degrees was performed in the manner of Table 3. The summation is not quite F_D/Z due to the numerical integration. The percent error induced by the numerical integration for a $d\beta$ of 2 degrees is:

$$\text{Percent error} = \frac{0.95106 - 0.95093}{0.95106} \times 100$$

Error = 0.014%

The following important points should be noted:

a. The minus sign in the Cos $(90 - \beta_N)$ summation refers to the direction of the axial force component.

b. The axial force summation is independent of the suspension-line force, F_l, the load-line inflated shape, and the parachute diameter.

Conclusion:

This approach to normal force distribution is reasonable because it meets the criteria of the aerodynamic drag force being equal to the summation of the normal force components along the load line.

DETERMINATION OF THE FORCE TANGENT TO THE BILLOWED CLOTH AT THE LOAD LINE

Now that the force per unit length along the load line has been determined as a function of β_N, the force, F_T, tangent to the billowed cloth at the

TABLE 3. NUMERICAL INTEGRATION OF AXIAL FORCE

β_N	Cos $(90-\beta_N)$	ΣCos $(90-\beta_N)$
17	0.29237	0.29237
15	0.25882	0.55119
13	0.22495	0.77614
11	0.19081	0.96695
9	0.15643	1.12339
7	0.12187	1.24525
5	0.08716	1.33241
3	0.05234	1.38475
1	0.01745	1.40220
-1	-0.01745	1.38475
-3	-0.05234	1.33241
-5	-0.08716	1.24526
↓	↓	↓
-85	-0.99619	-25.24867
-87	-0.99863	-26.24730
-89	-0.99985	-27.24715

load line can be resolved. The canopy is reintroduced to the analysis and the canopy geometry is illustrated in Figure 9 for an arbitrary point (X_N, Y_N, β_N). The plane of analysis passes through the arbitrary point perpendicular to the slope of β_N and passes through the parachute center line. At the point X_N, Y_N the force balance is:

$$2F_T \cos\phi = \frac{\Sigma F_N}{d\ell}$$

$$F_T = \frac{\Sigma F_N}{2d\ell \cos\phi} \quad \frac{lb}{in} \tag{10}$$

MINIMUM TANGENTIAL FORCE

Inspection of Equation (10) shows that the tensile force in the cloth, F_T, decreases as ϕ approaches 0 degree, and is a minimum at $\phi = 0°$. The angle ϕ is a function of ψ, ψ', θ and β_N, with reference to the geometry of the section through X_N, Y_N, at β_N of Figure 9.

$$\phi = 90 - \tau$$

$$\tau = \theta - \psi'$$

$$\phi = 90 - \theta + \psi' \tag{11}$$

therefore

when

$$\phi = 0$$

$$\theta = 90 + \psi' = \theta' \tag{11a}$$

To find ψ'

$$f = Y_N \sin\psi \tag{12}$$

$$f = A \sin\psi' \tag{12a}$$

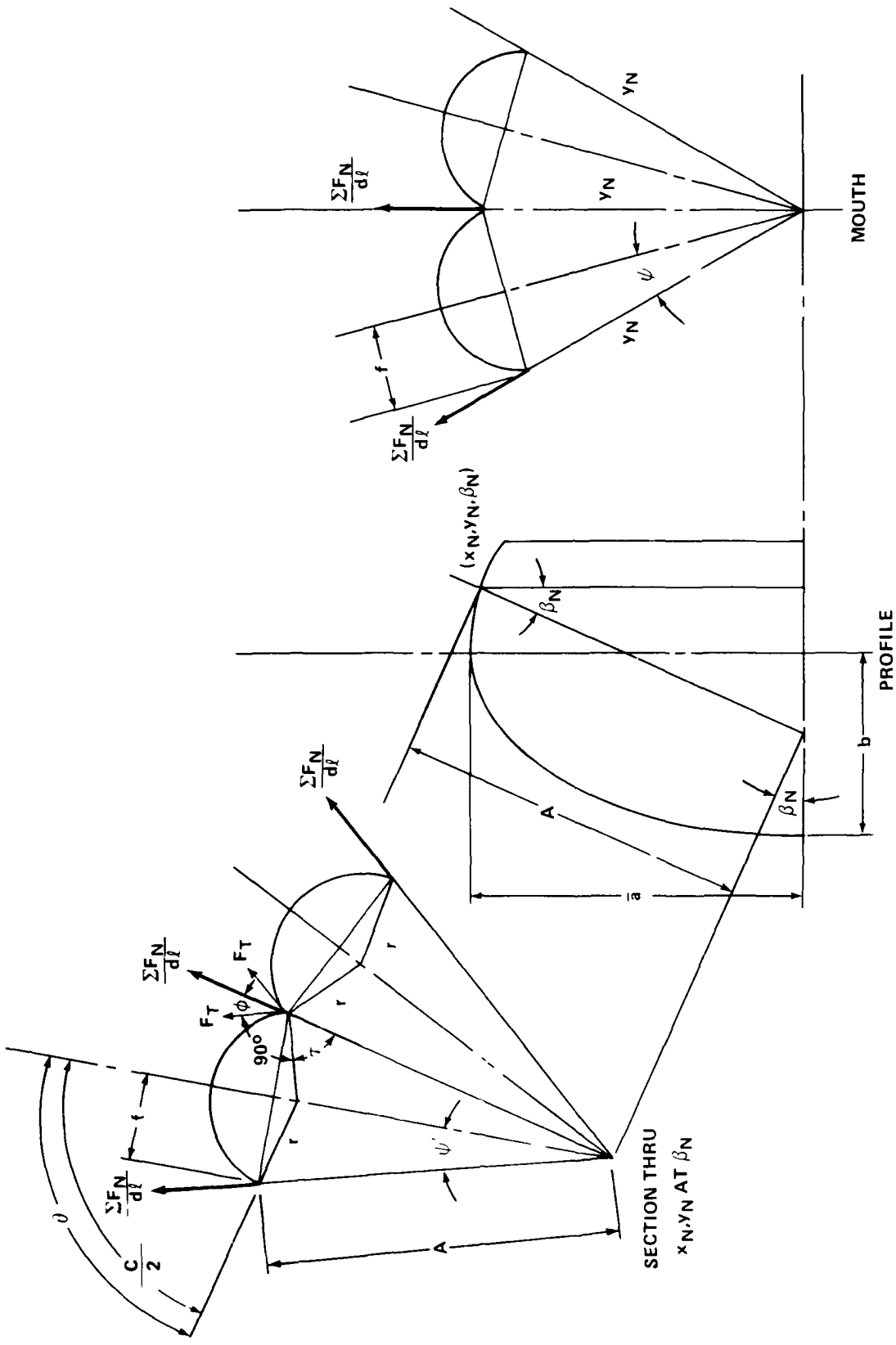

FIGURE 9. BILLOWED GORE GEOMETRY FOR AN ARBITRARY POINT ON THE LOAD LINE

where

$$A = \frac{Y_N}{Cos\beta_N} \tag{12b}$$

$$\frac{Y_N sin\psi'}{Cos\beta_N} = Y_N sin\psi$$

$$Sin\psi' = Sin\psi Cos\beta_N \tag{13}$$

$$\psi' = sin^{-1}(Sin\ \psi\ Cos\ \beta_N) \tag{13a}$$

and ψ is a function of the number of gores in the parachute.

$$2\psi = \frac{360°}{Z}$$

$$\psi = \frac{180°}{Z}$$

$$\psi' = sin^{-1}\ (sin\frac{180}{Z}Cos\beta_N) \tag{13b}$$

At the condition of $\emptyset$ = 0 degree, the inflated gore geometry is as shown in Figure 10. The billowed cloth in the gore is denoted by C'.

The theoretical shape of a "minimum cloth stress" gore design is compared to a conventional gore design in Figure 11 for a Flat Circular Parachute of D_o = 30 feet and 30 gores. The minimum stress configuration is based on the assumption that the profile shape of the gore mainseam remains unchanged, but realizing that the inflated shape may modify to a new profile. Use of cloth dimensions greater than C' are likely to cause a condition wherein the excess cloth between successive gores support each other and produce an area of large local radius of curvature as in Figure 12. Therefore, the optimum cloth angle is somewhat larger than 180°, as usually stated, by an additional $2\psi'$, and varies with location along the gore length. The properties of the "minimum cloth stress" gore design are illustrated in Figure 13.

In Figure 12, it was shown that excessive billow is undesirable. Therefore, a summary of the possible billow configurations and their effects upon design would be helpful.

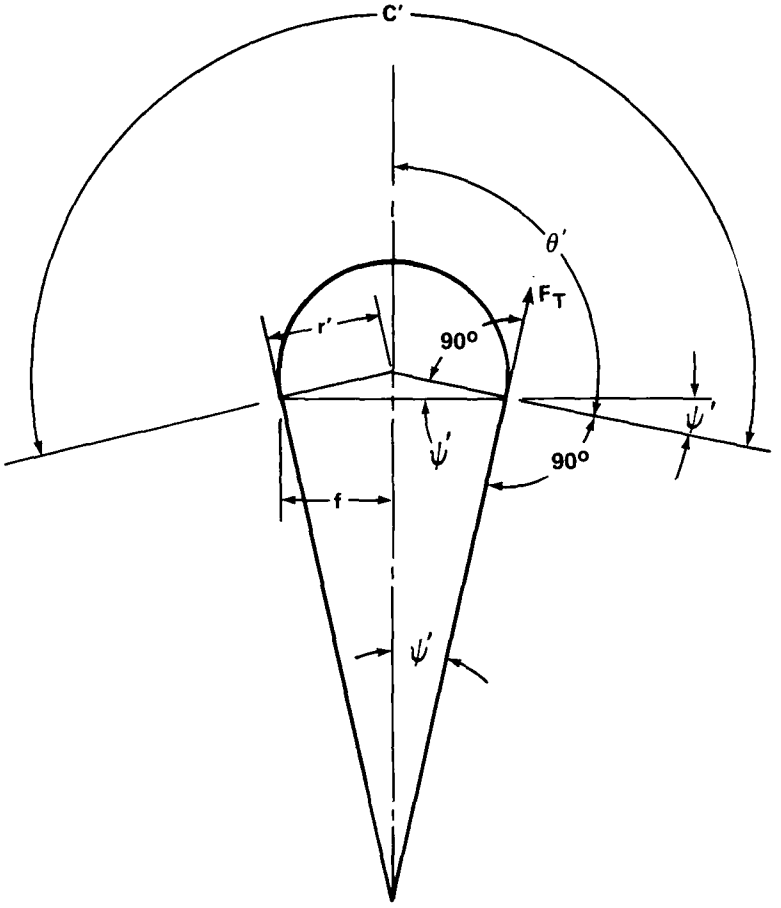

FIGURE 10. BILLOWED GORE GEOMETRY FOR MINIMUM STRESS

$$C' = 2r'\theta'$$

$$f = r'\text{Cos}\psi'$$

$$r' = \frac{f}{\text{Cos}\psi'}$$

$$C' = \frac{2f}{\text{Cos}\psi'}\left(\psi' + \frac{\pi}{2}\right) \qquad (14)$$

Where "f" comes from Equation (12)

The minimum force, F_T, is

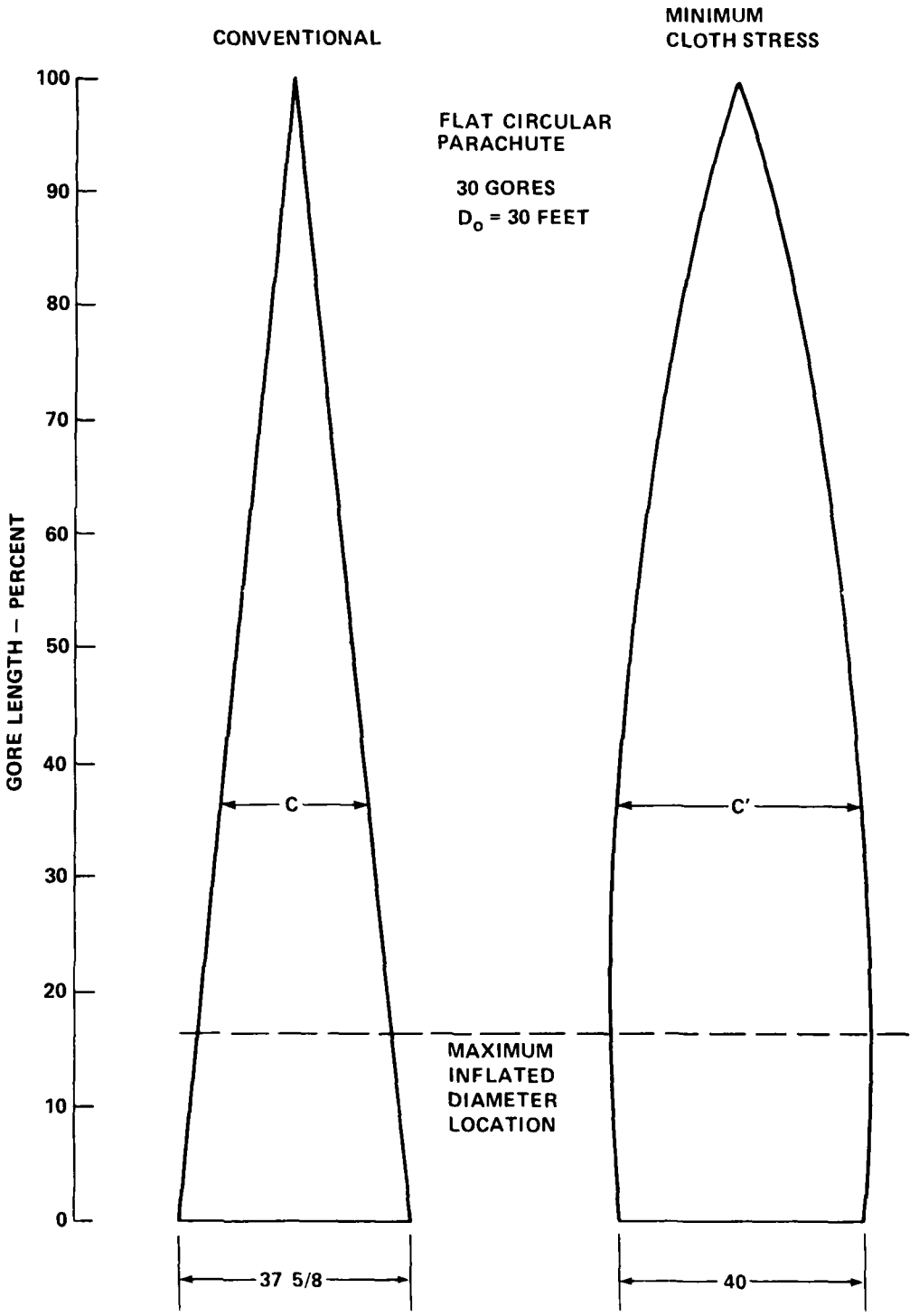

FIGURE 11. COMPARISON OF CONVENTIONAL FLAT CIRCULAR PARACHUTE GORE LAYOUT AND MINIMUM CLOTH STRESS GORE CONFIGURATION

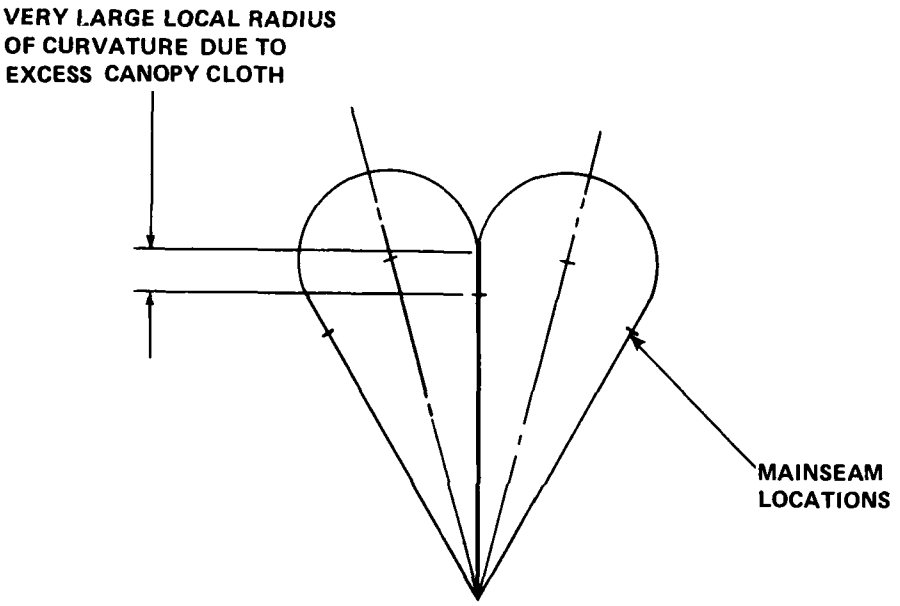

FIGURE 12. EFFECT OF EXCESS CLOTH BILLOW ON RADIUS OF CURVATURE

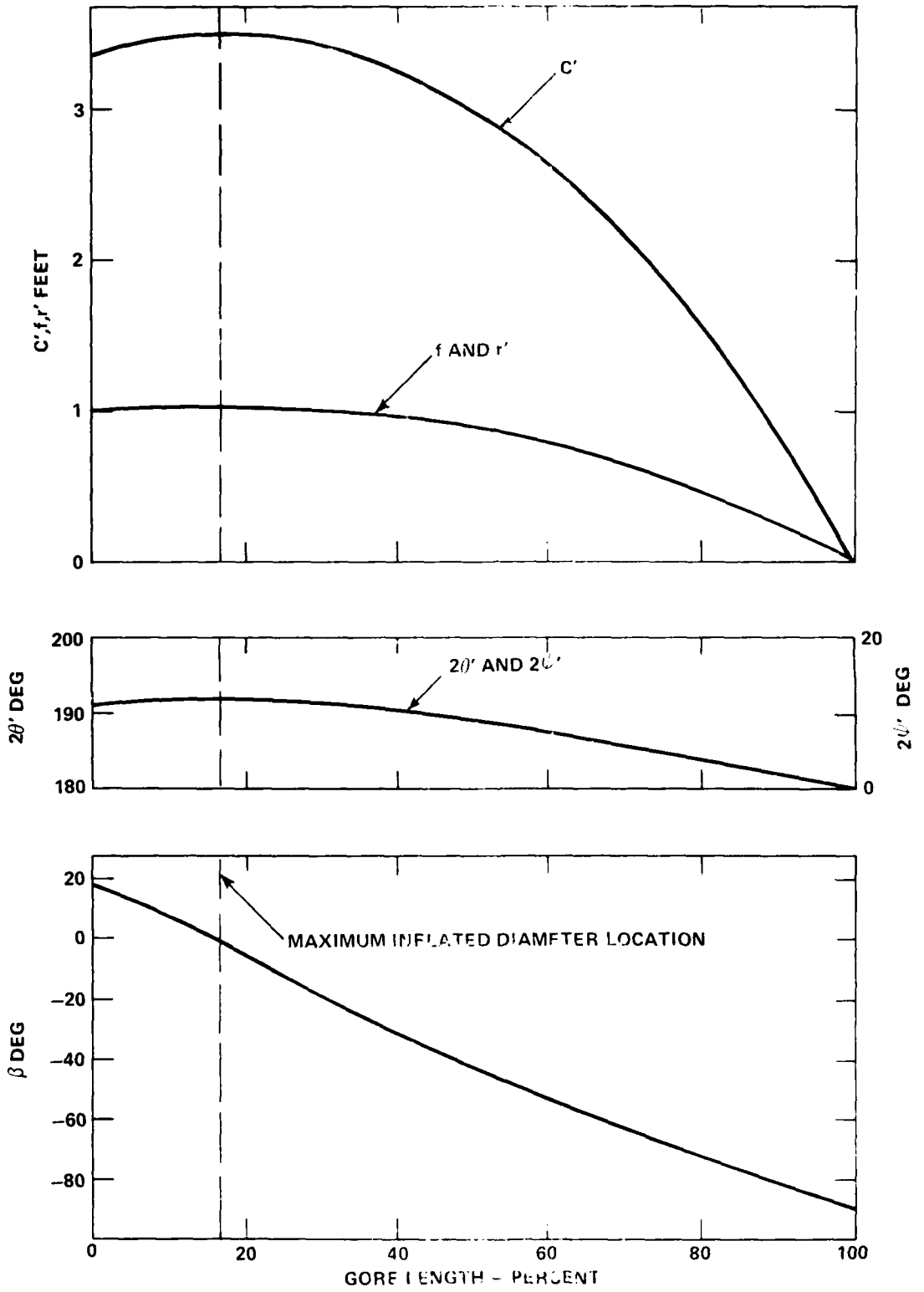

FIGURE 13. VARIATION OF MINIMUM CLOTH STRESS GORE GEOMETRY AS A FUNCTION OF GORE LENGTH

$$F_T = \frac{F_N}{2d\ell} \quad \frac{lb}{in} \tag{15}$$

At the arbitrary coordinates (X_N, Y_N, β_N) the width of the gore pattern C is known. This width can be compared to the theoretical gore widths required for $2\theta = 180$ degrees and $2\theta = 180 + 2\psi'$ degrees. Table 4 lists the possible configurations and effects. With reference to Figure 14

$$C = 2r\theta$$

when $2\theta = 180$ degrees $= \pi$ radians

then $r = f$

$$f = Y_N \sin\psi$$

$$C_{180} = \pi Y_N \sin\psi \tag{16}$$

TANGENTIAL FORCE IN THE CANOPY CLOTH AT AN ARBITRARY POINT ON THE LOAD LINE

The cloth tangent force, F_T, can be determined at any arbitrary point along the load line in the following manner:

a. Assume β_N

b. Calculate X_N from Equation 5, and Y_N from Equation 6.

c. Calculate the load-line arc length from the canopy vent or hem to the coordinates under study, from Equation 7 or 8.

d. Determine the gore width, C, from the gore pattern for the mainseam arc length determined in step c. See Figure 11.

Then with reference to Figure 9:

$$C = 2r\theta$$

$$f = r\sin\theta$$

$$\frac{C}{2f} = \frac{\theta}{\sin\theta} \tag{17}$$

where $f = Y_N \sin\frac{180}{Z}$ (12)

TABLE 4. BILLOW CONFIGURATIONS AND EFFECTS

CONFIGURATION	EFFECT
$C < C_{180}$	 RADIUS CENTER BELOW CHORD
$C = C_{180}$	 RADIUS CENTER ON CHORD
$C > C_{180}$	 RADIUS CENTER ABOVE CHORD
$C = C'$	MINIMUM CANOPY CLOTH STRESS
$C > C'$	EXCESS BILLOW CONDITION OF FIGURE 12
$C \leq 2f$	NO BILLOW HIGH CANOPY CLOTH STRESS

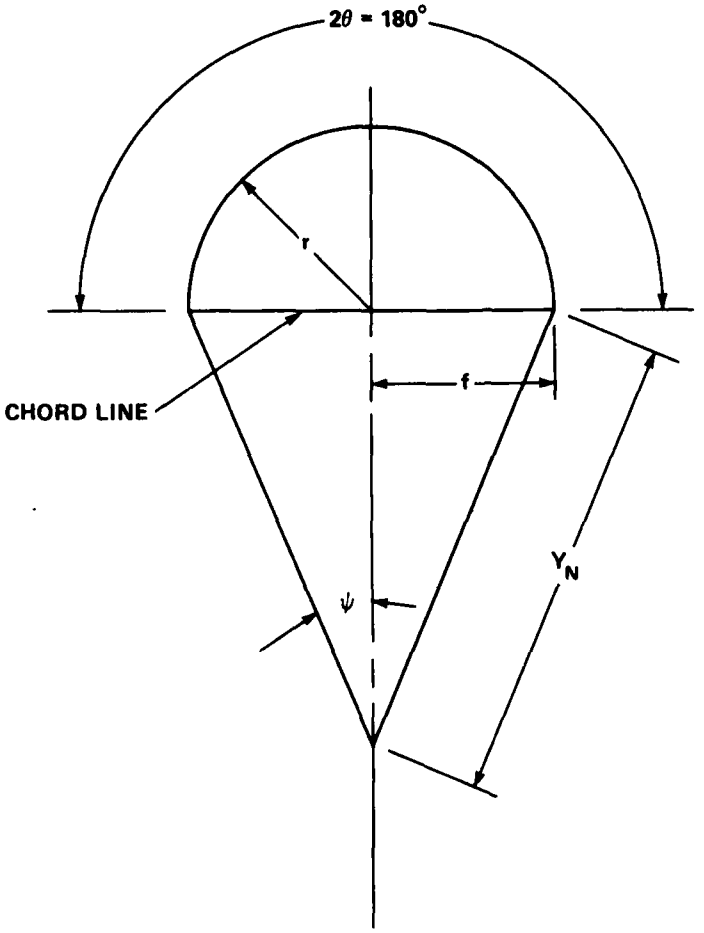

FIGURE 14. GORE BILLOW FOR 2θ = 180 DEGREES

and the angle θ is estimated from Figure 15. Vary θ from the estimated value until the calculated value of $\theta/\sin\theta = C/2f$.

therefore $$r = \frac{C}{2\theta} \tag{18}$$

$$\psi' = \sin^{-1}[\sin\frac{180}{Z}\ \text{Cos}\beta_N] \tag{13a}$$

then $$\phi = 90 - \theta + \psi' \tag{11}$$

$$\Sigma F_N = 2F_1 \sin\frac{d\beta}{2} \quad \text{lb} \tag{4}$$

$$\Sigma F_N = \frac{2F_D}{Z\text{Cos}\beta_o} \sin\frac{d\beta}{2} \quad \text{lb}$$

e. Calculate the arc length, $d\ell$, from $\beta_N - \frac{d\beta}{2}$ to $\beta_N + \frac{d\beta}{2}$ using the method of Equation 8.

$$F_T = \frac{\Sigma F_N}{2d\ell\text{Cos}\phi} \quad \frac{\text{lb}}{\text{in}} \tag{10}$$

Figure 16 is reproduced from Reference 4 and illustrates the shape and billow of an inflated gore. The increase in the angle ϕ at the various sections between the skirt hem and vent is evident. In the vent area the cloth tangent force can be greatly affected by large ϕ angles as shown in Figure 17. This points out the importance of canopy billow in the vent area.

Inflated canopies are sometimes seen to vibrate in that the adjacent mainseams spread apart and then approach each other. These excursions may be small, but are bound to have an effect on the cloth tangent force, especially in the vent area. The effects can be investigated by assuming a change in the central angle ψ by an increment $\pm d\psi$ and recalculating the resulting geometry and loads. Assume that the load-line inflated shape is constant, or appropriate changes in the load-line shape can be introduced.

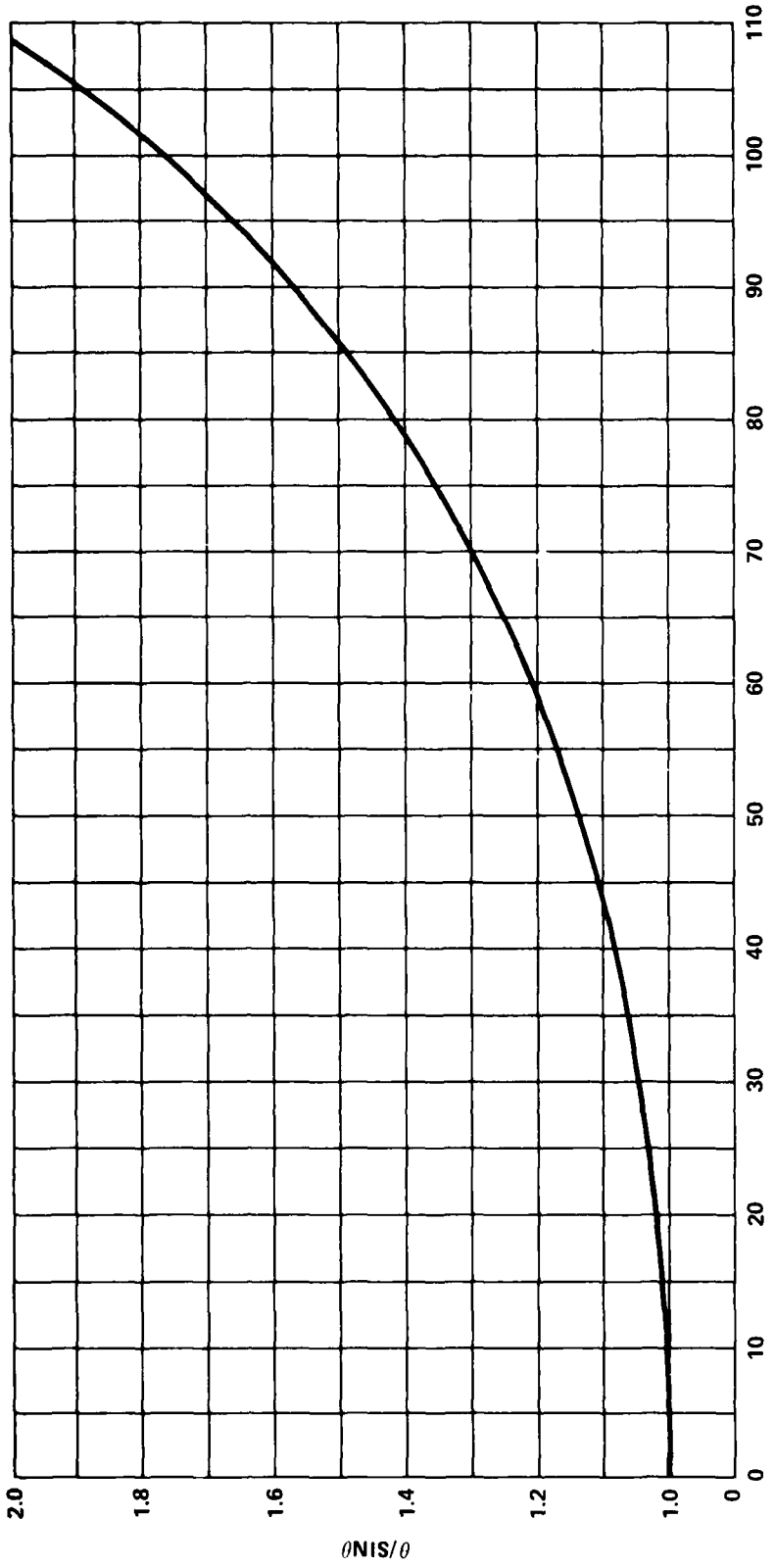

FIGURE 15. TRANSCENDENTAL EQUATION $\theta/\sin\theta$ SOLUTION AS A FUNCTION OF θ

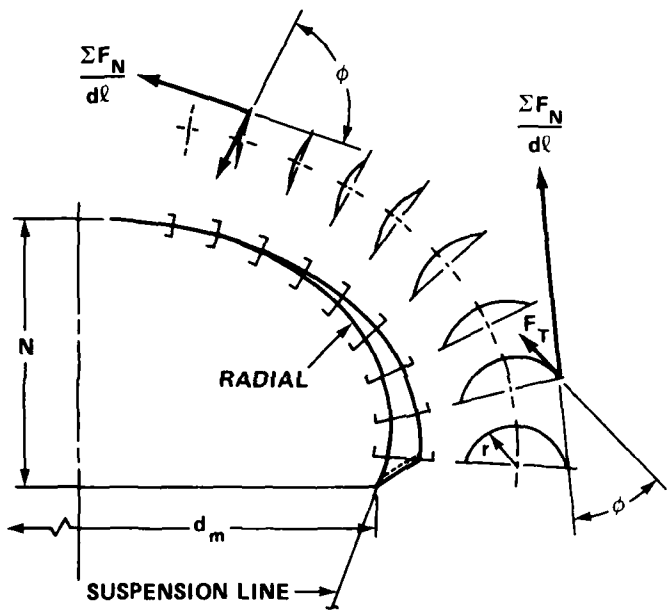

FIGURE 16. SHAPE OF AN INFLATED GORE REPRODUCED FROM REF. 4

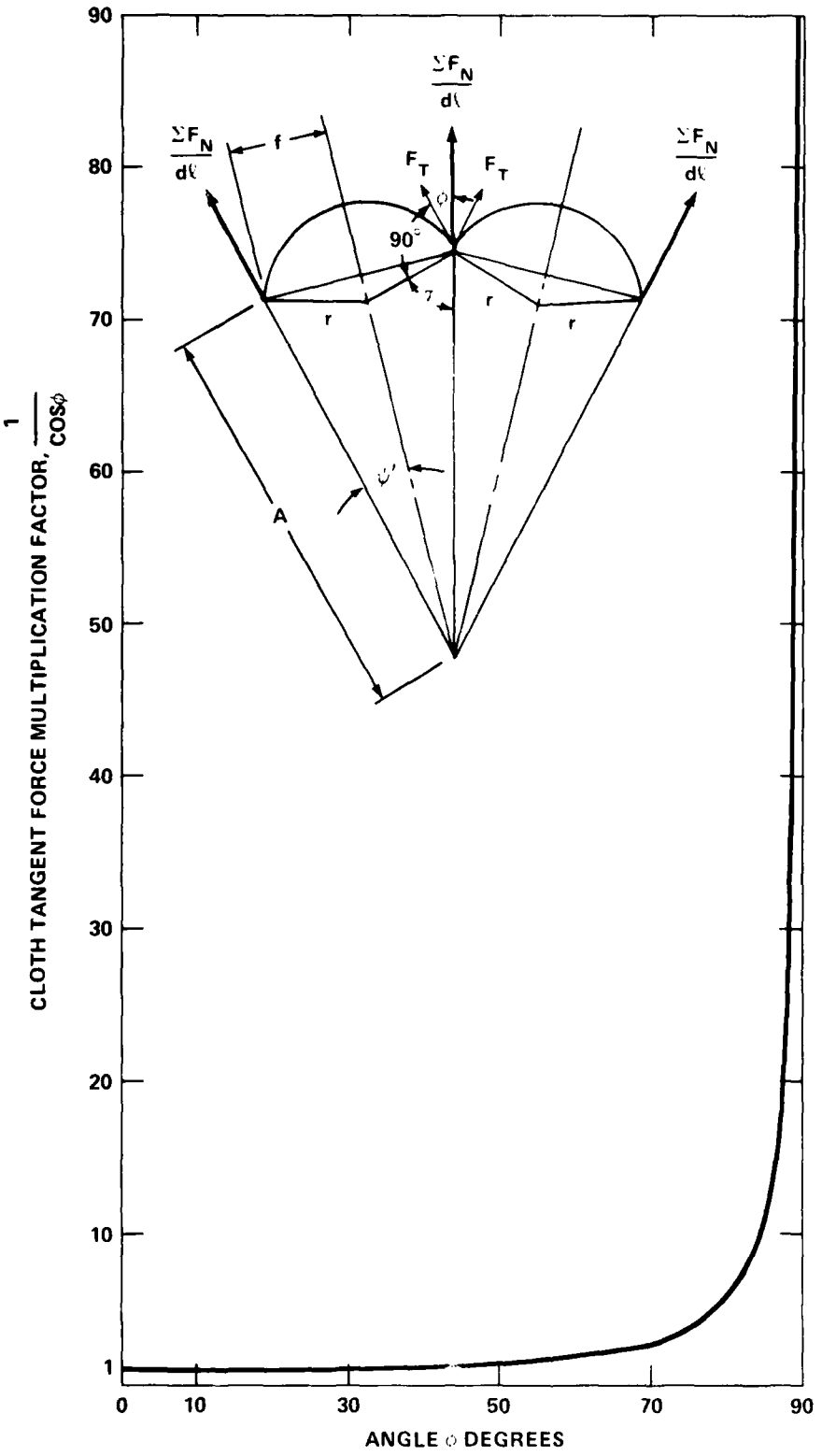

FIGURE 17. EFFECT OF ANGLE ϕ ON THE CLOTH TANGENTIAL FORCE STRESS

FORCE RESOLUTION IN THE CANOPY CLOTH OF SOLID CLOTH PARACHUTES

Solid cloth parachute canopies are usually constructed of gore sections which are either bias cut or block cut as shown in Figure 18. The magnitude of the force components resisted by the canopy cloth depends upon the geometric orientation of the warp and fill directions in the cloth relative to the force, F_T, which is tangent to the cloth. In the case of bias cut gores the force components are:

$$F_{c1} = F_T \sin \mu \tag{19}$$

$$F_{c2} = F_T \cos \mu \tag{20}$$

where $$\mu = 45° - \psi \tag{21}$$

and for block cut gores:

$$F_{c3} = F_T \text{ Cos } \psi \tag{22}$$

$$F_{c4} = F_T \sin \psi \tag{23}$$

While the force level in the cloth is dependent on a number of variables, it is also a function of the number of gores in the canopy. The variation of force levels due only to variations of the number of canopy gores is presented in Table 5.

TABLE 5. EFFECT OF THE NUMBER OF GORES ON THE CANOPY CLOTH FORCE LEVELS OF SOLID CLOTH PARACHUTES

FORCE LEVEL	NUMBER OF GORES		
	24	30	36
F_{C1}	$0.609F_T$	$0.629F_T$	$0.643F_T$
F_{C2}	$0.793F_T$	$0.777F_T$	$0.766F_T$
F_{C3}	$0.991F_T$	$0.994F_T$	$0.996F_T$
F_{C4}	$0.130F_T$	$0.104F_T$	$0.087F_T$

As the number of gores approaches infinity the apex angle ψ approaches zero and F_{C1} approaches F_{C2}. In the limit:

$$\psi = 0$$

$$F_{c1} = F_{c2} = F_T \sin (45-\psi) = 0.707 F_T$$

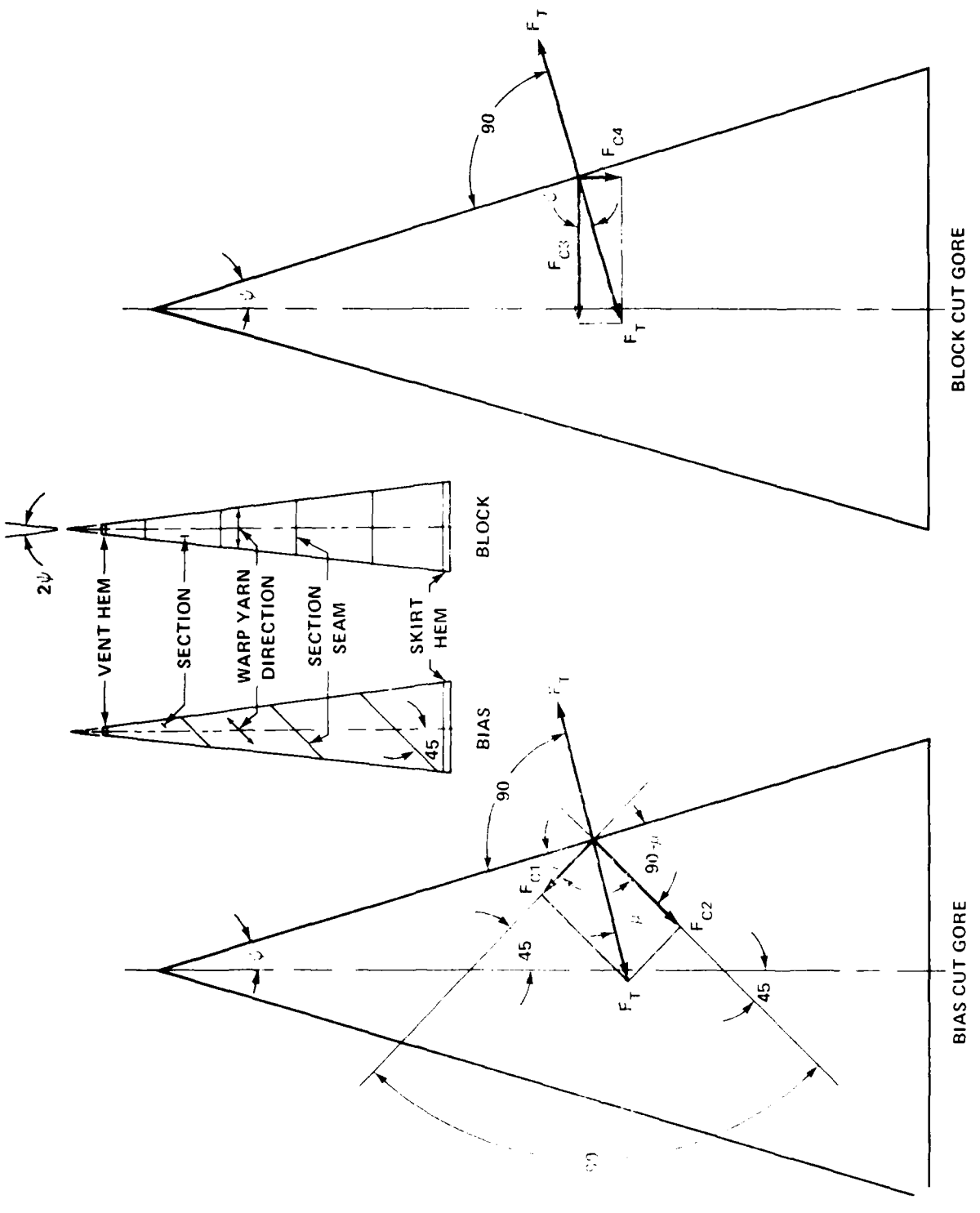

FIGURE 18. FORCE RESOLUTION IN THE CANOPY CLOTH

The force systems of Figure 18 are tangent to the billowed canopy cloth at the coordinates X_N, Y_N, β_N. Due to the multi-directions of curvature, the actual angles of the warp and fill directions to the load line may be distorted from the theoretical. The effects of angular distortions on stress variation may be examined by resolving the cloth tangent force, F_T, into two components at arbitrarily selected angles and the stress variation assessed. Care must be exercised not to assign unrealistic angular excursions.

FORCE RESOLUTION IN THE CANOPY CLOTH OF RING SLOT PARACHUTES

Figure 19 is a wind-tunnel test photograph of the 24-gore, 16-percent geometrically porous parachute of Table 2 at 200 miles per hour test velocity (q = 102.32 psf). With reference to Figures 19 and 20, the inflated parachute gore center line arc length is longer than the mainseam arc length. As designed the gore was flat and the gore center line length was actually shorter than the mainseam. This results in a wider spacing of the cloth rings along the gore center line and a subsequent rake angle, α, at the forward and rear hems of the rings.

At the arbitrary point X_N, Y_N, β_N the force F_T is tangent to the inflated cloth ring and must be resolved into two components F_R (the force in the ring) and F_t (a tearing force tangent to the mainseam).

A similar condition exists at the trailing hem of the circumferential ring, but the tangent force F_t is in opposition to the tangent force of the forward hem. Let the subscript F denote the forward edge of the circumferential ring and the subscript R denote the rear edge of the ring.

Then
$$F_{RF} = \frac{F_T}{\cos\alpha_F} \tag{27}$$

$$F_{tF} = F_T \tan\alpha_F \tag{28}$$

$$F_{RR} = \frac{F_T}{\cos\alpha_R} \tag{29}$$

$$F_{tR} = F_T \tan\alpha_R \tag{30}$$

The values of α_F and α_R plotted in Figure 21 were estimated by measuring the arc length of the Figure 19 parachute to determine the rake angles and angle locations as a function of ℓ/ℓ_T. For lack of any better data, the rake angle distribution of the 24-foot Ringslot Parachute versus ℓ/ℓ_T is assumed to be similar to the model parachute.

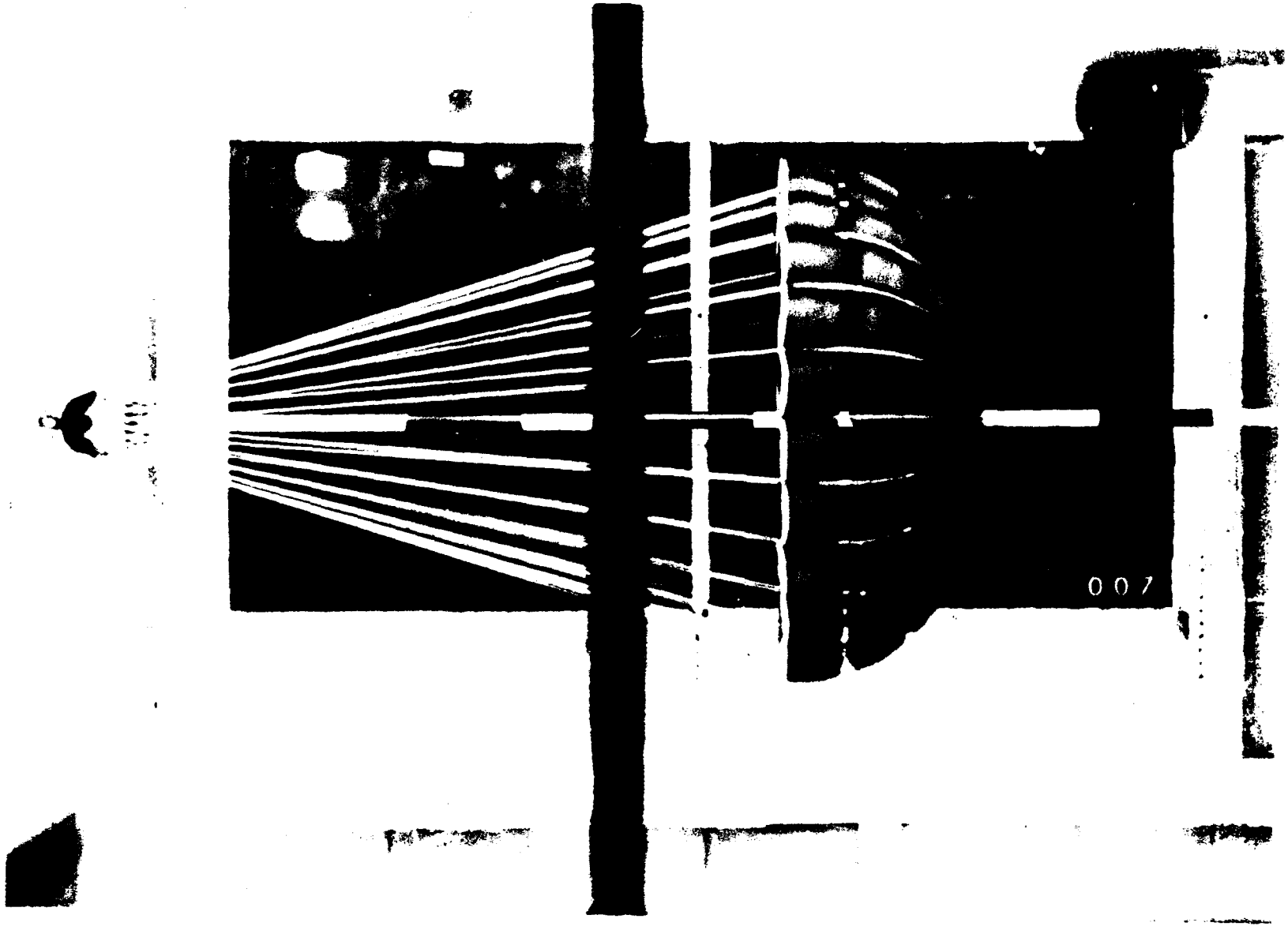

FIGURE 10. WIND TUNNEL TEST PHOTOGRAPH OF THE 24-GORE, 16 PERCENT GEOMETRICALLY POROUS PARACHUTE OF TABLE 2

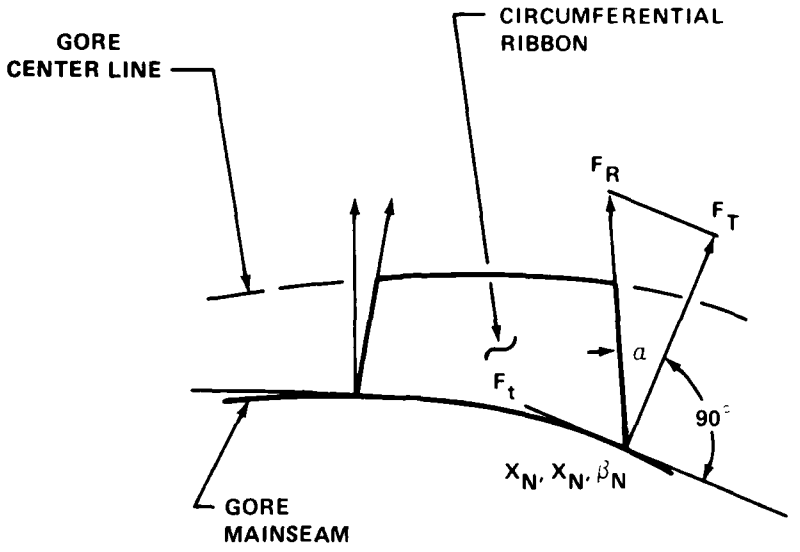

FIGURE 20. HEM FORCES IN A RINGSLOT PARACHUTE CIRCUMFERENTIAL RIBBON

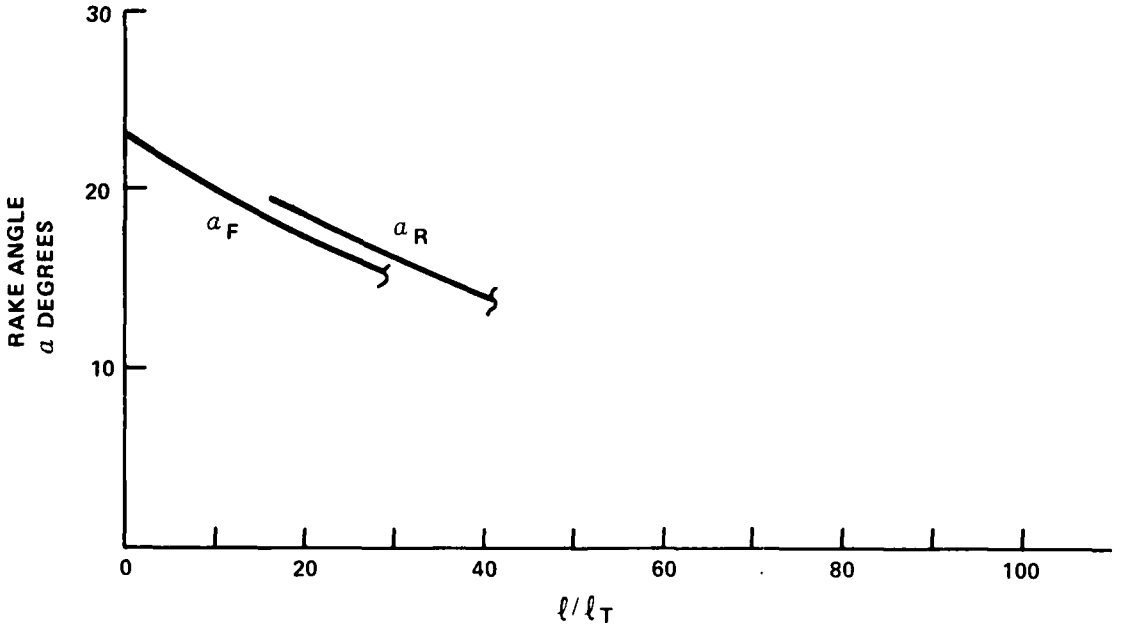

FIGURE 21. CIRCUMFERENTIAL RIBBON HEM RAKE ANGLES VERSUS PERCENT OF GORE LENGTH

COMMENTS ON WIND TUNNEL TESTING

The limited rake angle data of Figure 21 is caused by problems in placement of the camera during the test. The camera coverage for use in the original test purpose was adequate. However, attempting to use available coverage for other purposes, not envisioned at the time of the test, gives poor rake angle definition in the top three circumferential rings. In future tests where rake angle data is required two cameras would be used: One in the plane of the skirt hem and one in the plane of the vent, or some other approach which defines a true side view of the entire inflated parachute. This is also true of camera coverage of wind tunnel tests for all types of parachutes.

Data gathering on solid cloth types of parachutes can be enhanced by stripes of alternating colors woven into the canopy cloth, or printed on, during manufacture. These stripes of known width and orientation in the model provide improved definition of warp and fill direction angles in the inflated state. Striped patterns on radial reinforcement tapes would also be an aid in determining where circumferential rings are located in percent of gore length in the inflated state. This would minimize the discrepancies between inflated and constructed gore lengths. Measurement of the elongation of a suspended gore mainseam assembly subjected to static forces in the range of expected suspension-line forces before and after the test would also be beneficial.

EXAMPLE 1: STRESS ANALYSIS OF A 24-GORE RINGSLOT PARACHUTE OF 24-FOOT D_o DIAMETER

As an example of the stress analysis technique, a sample calculation is presented for a 24-foot D_o diameter, 24-gore Ringslot Parachute for conditions of 200 mph at sea level air density. The shape of the inflated steady state canopy is taken as similar to the 24-gore, 16-percent geometrically porous Ringslot Parachute of Table 2. The stress distribution of the unbillowed gore is to be determined, and the moderating effects of gore billow shall be compared.

The results of this analysis are summarized in Tables 6 and 7. The Table 6 summary consists of four sections (a) the canopy geometry, (b) the normal force per unit mainseam length, (c) the geometry, forces, and pressure coefficient distribution for the unbillowed gore, and (d) the geometry, forces, and pressure coefficient distribution for the billowed gore. The tensile forces in the circumferential ring hems and tearing forces are presented in Table 7.

Parachute surface area and drag area.

$$S_o = \frac{\pi}{4} D_o^2$$

$$S_o = \frac{\pi}{4} (24)^2$$

$$S_o = 452.3904 \text{ ft}^2$$

$$C_D S_o = 0.55 \times 452.3904$$

$$C_D S_o = 248.8147 \text{ ft}^2$$

TABLE 6. STRESS

LOCATION	β_N DEG	X_N IN. (5)*	Y_N IN. (6)	ℓ IN. Σ(8)	$d\ell$ IN. (8)	ℓ/ℓ_T	r IN. (12)
			CANOPY GEOMETRY				
SKIRT HEM	18.0	25.531	95.874	0	0	0.000	12.514
	17.9	25.391	95.920	0.147	0.293	0.001	12.520
	14.0	19.920	97.484	5.838	0.291	0.038	12.724
	10.0	14.261	98.687	11.624	0.288	0.076	12.881
	5.0	7.143	99.624	18.806	0.286	0.124	13.004
	0.1	0.143	99.936	25.816	0.286	0.170	13.044
MAX. INFLATED DIAMETER, $\beta_N = 0°$							
	-0.1	-0.059	99.936	26.017	0.117	0.171	13.044
	-5.0	-2.938	99.808	28.890	0.118	0.190	13.028
	-10.0	-5.897	99.417	31.886	0.121	0.210	12.977
	-20.0	-11.972	97.781	38.186	0.133	0.251	12.763
	-30.0	-18.405	94.764	45.300	0.154	0.298	12.369
	-40.0	-25.365	89.859	53.920	0.190	0.354	11.729
	-50.0	-32.958	82.209	64.618	0.246	0.425	10.730
	-55.0	-36.975	76.962	71.228	0.284	0.467	10.046
	-56.0	-37.791	75.774	72.669	0.293	0.4775	9.891
	-56.1	-37.873	75.653	72.815	0.293	0.4785	9.875
	-56.2	-37.955	75.531	72.926	0.294	0.4795	9.859
	-56.3	-38.037	75.408	73.110	0.295	0.4804	9.843
	-60.0	-41.080	70.503	78.883	0.330	0.518	9.203
	-65.0	-45.174	62.618	87.770	0.382	0.577	8.173
	-70.0	-49.096	53.120	98.050	0.441	0.644	6.934
	-75.0	-52.619	41.912	109.802	0.499	0.722	5.471
	-80.0	-53.457	29.068	122.560	0.552	0.808	3.794
	-84.9	-57.289	15.199	136.954	0.588	0.900	1.984
VENT HEM	-87.5	-57.799	7.502	144.669	0.598	0.9507	0.979

* THE NUMBER IN THE PARENTHESIS CORRESPONDS TO THE NUMB

D_o = 24 FT
$C_D S_o$ = 81 FT^2
$\bar{a}$ = 99.936 IN.
b = 57.963 IN.
b' = 90.472 IN.
N = 80.848 IN.

37/38

14/3

STRESS ANALYSIS SUMMARY OF THE 24-FOOT, 24-GORE, RINGSLOT PARACHUTE OF EXAMPLE 1

		NORMAL FORCE	UNBILLOWED GORE							BILLOWED G			
f	ψ	$\Sigma F_N/d\ell$	C	Θ	r	ϕ	$\frac{1}{\cos\phi}$	F_T	CP	C_B	Θ_B	r_B	ϕ
IN. (12)	DEG (13a)	LE/IN.	IN. (24)	DEG (17)	IN. (18)	DEG (11)		LB/IN. (10)	(33)	IN. (25)	DEG (17)	IN. (18)	DEG (11)
2.514	7.131	–	37.916	86.65	12.536	10.481	1.0170	–	–	37.916	86.65	12.536	10.481
2.520	7.135	13.270	37.878	86.51	12.544	10.620	1.0174	6.751	0.758	37.879	86.52	12.543	10.615
2.724	7.276	13.402	36.460	81.11	12.879	16.166	1.0412	6.977	0.763	36.509	81.25	12.874	16.030
?.881	7.385	12.509	35.019	75.36	13.313	22.025	1.0787	7.286	0.770	35.117	75.68	13.294	21.705
3.004	7.471	13.594	33.230	67.77	14.048	29.701	1.1513	7.825	0.784	33.388	68.39	13.986	29.079
3.044	7.500	13.618	31.485	59.72	15.105	37.780	1.2652	8.615	0.803	31.703	60.76	14.950	36.745
.044	7.500	33.162	31.432	59.46	15.145	38.040	1.2697	21.053	1.957	31.651	60.51	14.987	36.992
3.028	7.471	32.938	30.716	56.01	15.712	41.461	1.3344	21.976	1.969	30.959	57.28	15.484	40.189
?.977	7.385	32.176	29.973	52.50	16.356	44.885	1.4114	22.706	1.954	30.241	54.05	16.030	48.335
.763	7.045	29.383	28.403	45.39	17.928	51.655	1.6119	23.681	1.859	28.724	47.66	17.267	49.385
.369	6.491	25.265	26.628	37.82	20.172	58.671	1.9232	24.295	1.695	27.010	41.25	18.762	55.246
.729	5.739	20.512	24.505	29.21	24.035	66.529	2.5107	25.750	1.508	24.958	34.75	20.579	60.992
.730	4.813	15.822	21.817	18.00	34.725	76.813	4.3834	34.688	1.406	22.361	28.35	22.597	66.463
.046	4.294	13.704	20.205	10.64	54.407	83.654	9.0465	61.986	1.604	20.804	26.14	22.802	68.155
.891	4.186	13.306	19.811	5.58	101.718	88.606	41.0969	273.412	3.783	–	–	–	–
.875	4.175	13.270	19.773	5.02	112.849	89.155	67.7921	449.782	5.610	–	–	–	–
.859	4.164	13.229	19.735	4.38	129.090	89.784	265.2304	1754.351	13.590	–	–	–	–
.843	4.153	13.189	19.701	4.11	137.199	90.039	1465.539	9664.166	99.142	–	–	–	–
203	3.742	11.812	18.260	–	–	–	–	–	–	18.924	23.38	23.190	70.362
173	3.162	10.181	16.046	–	–	–	–	–	–	16.785	22.77	21.118	70.392
934	2.559	8.838	13.487	–	–	–	–	–	–	14.312	24.89	16.474	67.669
471	1.936	7.797	10.541	–	–	–	–	–	–	11.480	30.65	10.731	61.286
794	1.299	7.059	7.280	–	–	–	–	–	–	8.315	42.07	5.663	49.232
984	0.665	6.626	3.792	–	–	–	–	–	–	4.945	64.38	2.200	26.282
979	0.326	6.511	1.869	–	–	–	–	–	–	3.087	90.33	0.979	0.0

NUMBER OF THE FORMULA USED TO CALCULATE THE DESIGNATED VARIABLE

IN. R_C = 144 IN. β_o = 18° $\Sigma F_N/F_1$ = 0.003491

N. R_B = 149.035 IN. ψ = 7.5°

N. C_H = 37.916 IN. γ = 7.249° F_1 = 1115.227 LB.

N. T = 145.243 IN.

2 of 3

T PARACHUTE OF EXAMPLE 1

RE			BILLOWED GORE						
$\frac{1}{\cos\phi}$	F_T LB/IN. (10)	CP (33)	C_B IN. (25)	Θ_B DEG (17)	r_B IN. (18)	ϕ DEG (11)	$\frac{1}{\cos\phi}$	F_T LB/IN. (10)	CP (33)
1.0170	–	–	37.916	86.65	12.536	10.481	1.0170	–	–
1.0174	6.751	0.758	37.879	86.52	12.543	10.615	1.0174	6.521	0.732
1.0412	6.977	0.763	36.509	81.25	12.874	16.030	1.0405	6.972	0.762
1.0787	7.286	0.770	35.117	75.68	13.294	21.705	1.0763	7.266	0.769
1.1513	7.825	0.784	33.388	68.39	13.986	29.079	1.1442	7.777	0.783
1.2652	8.615	0.803	31.703	60.76	14.950	36.745	1.2480	8.497	0.800
1.2697	21.053	1.957	31.651	60.51	14.987	36.992	1.2520	20.760	1.950
1.3344	21.976	1.969	30.959	57.28	15.484	40.189	1.3090	21.559	1.960
1.4114	22.706	1.954	30.241	54.05	16.030	48.335	1.3748	22.119	1.942
1.6119	23.681	1.859	28.724	47.66	17.267	49.385	1.5362	22.569	1.840
1.9232	24.295	1.695	27.010	41.25	18.762	55.246	1.7542	22.160	1.662
2.5107	25.750	1.508	24.958	34.75	20.579	60.992	2.0621	21.149	1.447
3.3834	34.688	1.406	22.361	28.35	22.597	66.463	2.5041	19.815	1.234
5.0465	61.986	1.604	20.804	26.14	22.802	68.155	2.6874	18.414	1.137
10.0969	273.412	3.783	–	–	–	–	–	–	–
28.7921	449.782	5.610	–	–	–	–	–	–	–
82.2304	1754.351	13.590	–	–	–	–	–	–	–
289.539	9664.166	99.142	–	–	–	–	–	–	–
	–	–	18.924	23.38	23.190	70.362	2.9755	17.573	1.067
	–	–	16.785	22.77	21.118	70.392	2.9799	15.169	1.011
	–	–	14.312	24.89	16.474	67.669	2.6318	11.630	0.994
	–	–	11.480	30.65	10.731	61.286	2.0814	8.115	1.064
	–	–	8.315	42.07	5.663	49.232	1.5314	5.405	1.344
	–	–	4.945	64.38	2.200	26.282	1.1153	3.695	2.3637
	–	–	3.087	90.33	0.979	0.0	1.0000	3.255	4.679

ED VARIABLE

F_1 = 0.003491

F_1 = 1115.227 LB.

3 of 3

TABLE 7. TENSILE FORCES IN THE HEM OF THE CIRCUMFERENTIAL RINGS AND TEARING FORCES AT THE GORE MAINSEAM OF THE RINGSLOT PARACHUTE OF EXAMPLE 1.

R	ℓ/ℓ_T	F_T * lb/in (10)†	α_F ** DEG	F_{RF} lb/in (27)	F_{tF} lb/in (28)	α_R ** DEG	F_{RR} lb/in (29)	F_{tR} lb/in (30)
0	0	6.5	23	7.06	2.76			
19	.132	7.86				20.4	8.39	2.92
22.043	.153	8.19	16.75	8.55	2.45			
41.043	.285	22.33				13.7	22.98	5.44
44.086	.306	RAKE ANGLE DATA UNAVAILABLE						
63.086	.438							

* FROM FIGURE 27 FOR BILLOWED GORE CONFIGURATIONS

** FROM FIGURE 21

† NUMBERS IN THE PARENTHESES CORRESPONDS TO THE EQUATION USED TO CALCULATE THE DESIGNATED VARIABLE

Dynamic pressure and parachute drag force at 200 mph.

$$q = \frac{1}{2}\rho V^2$$

$$q = \frac{0.002378}{2} (293)^2$$

$$q = 102.31 \text{ lb/ft}^2$$

$$F_D = q\ C_D S_o$$

$$F_D = 102.31 \times 248.8147$$

$$F_D = 25456.2340 \text{ lb}$$

Suspension line force, F_l

$$\beta_o = 18° \text{ (measured from Figure 19)}$$

$$F_l = \frac{F_D}{Z \cos \beta_o}$$

$$F_l = \frac{25456.2340}{24 \times \cos 18°}$$

$$F_l = 1115.2612 \text{ lb}$$

$$R_c = \frac{Do}{2}$$

$$R_c = \frac{24}{2} \times 12$$

$$R_c = 144 \text{ inches}$$

$$\psi = \frac{360}{2Z}$$

$$\psi = \frac{360}{2 \times 24}$$

$$\psi = 7.5°$$

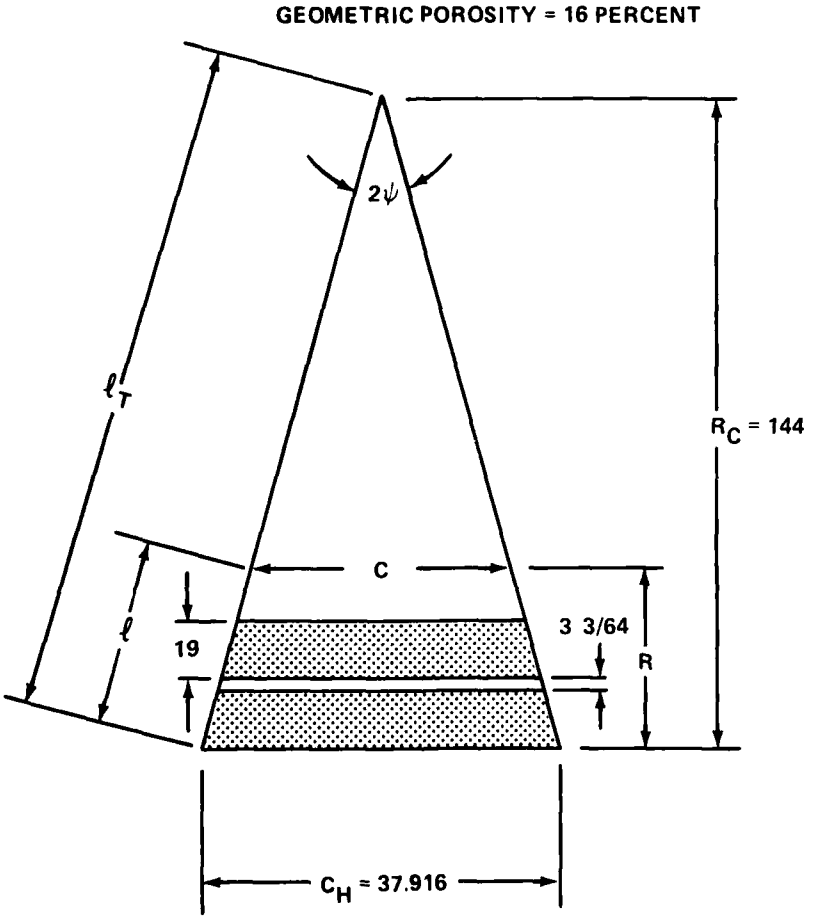

FIGURE 22. UNBILLOWED GORE GEOMETRY FOR THE RINGSLOT PARACHUTE OF EXAMPLE 1

With reference to Figure 22.

$$C_H = 2R_c \tan\psi$$

$$C_H = 2x144\tan 7.5°$$

$$C_H = 37.9159 \text{ inches}$$

$$\ell_T = \frac{R_C}{\text{Cos } \psi}$$

$$\ell_T = \frac{144}{\text{Cos } 7.5°}$$

ℓ_T = 145.2426 inches nominal unstressed gore mainseam length.

Determination of the unbillowed gore widths as a function of the ℓ/ℓ_T ratio.

The mainseam arc length calculations are summed from the canopy hem to the canopy vent. Therefore:

$$\frac{C}{C_H} = \frac{R_C - R}{R_C} = \frac{\ell_T - \ell}{\ell_T}$$

$$\frac{C}{C_H} = 1 - \frac{\ell}{\ell_T}$$

$$C = C_H \left(1 - \frac{\ell}{\ell_T}\right) \tag{24}$$

Determination of the inflated canopy arc length, ℓ_T, and arc length ratio ℓ/ℓ_T.

$$X = \frac{-b}{\sqrt{1 + \frac{1}{\tan^2 ß}\left(\frac{\bar{a}}{-b}\right)^2}} \tag{5}*$$

$$Y = \pm \bar{a}\sqrt{1 - \left(\frac{x}{-b}\right)^2} \tag{6}*$$

*When x>0 use b' in calculations. When x<0 use (-b).

$$d\ell = \sum_{X_1}^{X_2} \sqrt{\left(X_2-X_1\right)^2+\left(Y_2-Y_1\right)^2} \qquad (8)$$

From Table 2 the inflated parachute shape parameters are:

$$\frac{2\bar{a}}{D_o} = 0.694;\ \frac{b}{\bar{a}} = 0.580;\ \frac{b'}{\bar{a}} = 0.9053;\ \frac{N}{\bar{a}} = 0.809$$

For a D_o = 24 feet

$\bar{a}$ = 99.936 inches; b = 57.9629 inches; b' = 90.4721 inches; N = 80.8482 inches.

Equations 5, 6, and 8 were programmed to calculate X, Y, ℓ, and ℓ/ℓ_T for selected β_N angles from the canopy hem to the vent. The effect of varying the value of $d\beta/2$ on the calculated accuracy of ℓ_T for various $d\beta/2$ iterations was analyzed by assigning $d\beta/2$ values of 0.1, 0.5, 1.0, 2.0 and comparing the resulting values of ℓ_T. The accuracy of the four determinations of arc length can be judged by their differences as listed in Table 8. Arc lengths calculated for $d\beta/2=2°$ are accurate to the second decimal compared to the arc length calculated for $d\beta/2=0.1°$.

TABLE 8. ACCURACY OF ARC LENGTH CALCULATIONS FOR VARIOUS VALUES OF $d\beta/2$

$d\beta/2$ DEG.	ℓ_T INCHES	ℓ_T FOR $\frac{d\beta}{2} = 0.1 - \ell_T$ FOR $\frac{d\beta}{2}$
0.1	152.1727	0.0000
0.5	152.1722	0.0005
1.0	152.1708	0.0014
2.0	152.1650	0.0077

The angle ϕ is an important parameter in the stress analysis since it denotes a stress concentration factor which determines the maximum cloth stress. The canopy vent is the most likely maximum stress location and occurs at $\ell/\ell_T = 0.9507$ in the example.

Then $$C_V = C_H \left(1 - \frac{\ell}{\ell_T}\right) \tag{24}$$

$$C_V = 37.9159\ (1 - .9507)$$

$$C_V = 1.8692 \text{ in}$$

and $$f = Y_N \sin \psi \tag{12}$$

$$f = 7.5017 \sin 7.5°$$

$$f = 0.9792 \text{ in}$$

$$\frac{C_V}{2f} = 0.9545$$

Values of C/2f of less than 1.00 indicate a high stress condition. Other high stress indicators are the reduction of the gore billow angle θ to zero degree which results in an infinite local radius of curvature, or, from equation (11), the angle ϕ becomes 90 degrees when $\theta = \psi'$ and $1/\text{Cos } 90° = \infty$.

$$\phi = 90 - \theta + \psi' \tag{11}$$

For the unbillowed gore of example 1 the infinite radius, $\theta = 0°$, condition occurs at a $\beta_N = 56.6$ degrees, and the $\phi = 90°$ condition occurs at $\beta_N = -56.3$ degrees.

The need for addition of billow to the gore to reduce cloth stress to a manageable level has been established, and the next step is to determine the amount of billow to be provided. The maximum allowable billow C' is:

$$C'_V = \frac{2f}{\text{Cos}\psi'} \left(\psi' + \frac{\pi}{2}\right) \tag{14}$$

$$\psi' = \sin^{-1}[\sin\psi \ \text{Cos}\beta_N] \tag{13a}$$

from the arc length calculations $\ell/\ell_T = 0.9507$ occurs at a $\beta_N = -87.5°$, $Y_N = 7.5017$ in

$$\psi' = \sin^{-1}[\sin 7.5 \text{ Cos } -87.5]$$

$$\psi' = 0.3262 \text{ degree}$$

$$f = Y_N \sin \psi$$

$$f = 7.5017 \sin 7.5$$

$$f = 0.9792 \text{ in.}$$

$$C_V' = \frac{2x.9792}{\text{Cos } 0.3262} \left(\psi' + \frac{\pi}{2}\right)$$

$$C_V' = 3.0871 \text{ in.}$$

and the local radius of curvature

$$r = \frac{c'}{2\theta}$$

$$r = \frac{3.0871x57.3}{2x90.3262}$$

$$r = 0.9792 \text{ in.}$$

The ratio of billowed to unbillowed gore width at the vent is:

$$\frac{C'_V}{C_V} = \frac{3.0871}{1.8692}$$

$$\frac{C'_V}{C_V} = 1.6516$$

The unbillowed gore can be restructured to a billowed configuration as shown in Figure 23.

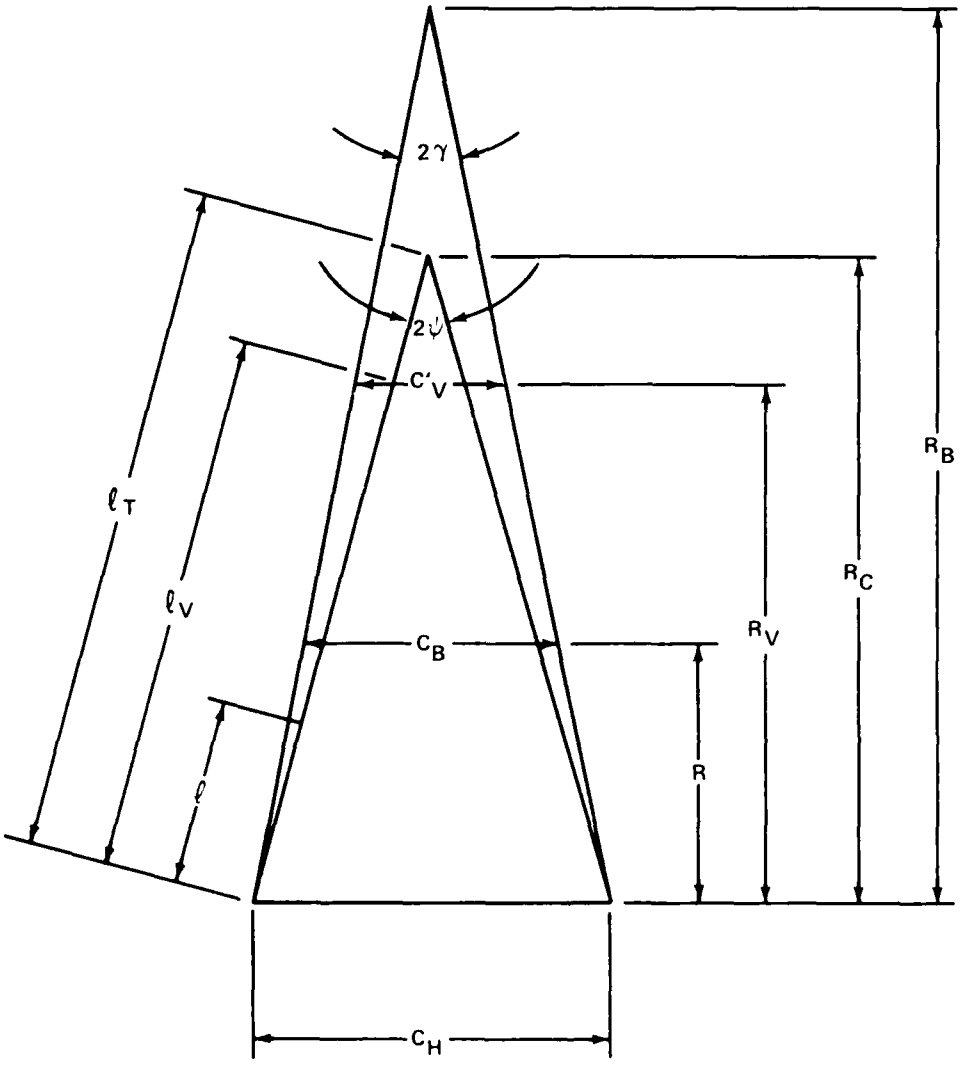

FIGURE 23. BILLOWED GORE GEOMETRY FOR THE RINGSLOT PARACHUTE OF EXAMPLE 1

$$\tan\gamma = \frac{C_H - C'_V}{2\ R_V} = \frac{C_H}{2R_B} = \frac{C'_V}{2(R_B - R_V)}$$

when $C_V = C'_V$

$$\tan\ \gamma = \frac{37.9159-3.0871}{2x144x.9507}$$

$$\tan\ \gamma = 0.1272$$

$$\gamma = 7.2493°$$

$$R_B = \frac{C_H}{2\tan\gamma}$$

$$R_B = \frac{37.9159}{2x0.1272}$$

$$R_B = 149.0352 \text{ inches}$$

$$\tan\ \gamma = \frac{C_B}{2(R_B-R)}$$

$$R = R_C\ \frac{\ell}{\ell_T}$$

$$R_B - R = \frac{C_B}{2\tan\gamma}$$

$$C_B = 2(R_B-R)\ \tan\gamma$$

$$C_B = 2\left(R_B - R_C\ \frac{\ell}{\ell_T}\right)\tan\gamma \qquad (25)$$

In the computation of the mainseam normal force per unit length, the local arc length $d\ell$ is the particular gore length from $\beta_N - \frac{d\beta}{2}$ to $\beta_N + \frac{d\beta}{2}$

The geometry, force, and pressure coefficients for the billowed and unbillowed gores were calculated for various β_N from the canopy hem to vent and listed in Table 6. The several variables were calculated by means of the formulas listed in parenthesis in each column. The order of calculation is the same as the order of presentation. Graphs of the several variables as related to percent of the gore length are illustrated in Figures 24 throug 28 for billowed and unbillowed gore designs. The affect of gore billow on stress relief is clearly illustrated.

CANOPY PRESSURE DISTRIBUTION

An advantage of the load-line approach to canopy force analysis is that it presents an opportunity to estimate a theoretical static pressure distribution over the canopy surface. This approach is called a static pressure distribution because it does not include the dynamic effects of fluttering cloth, canopy oscillations, or changing air flow patterns due to canopy inflation.

THE FULLY INFLATED STEADY STATE

The preceding force analysis resolved the parachute drag force, F_D, into components which were tangent, F_l, and normal, ΣF_N, to the load line. The stress tangent to the canopy cloth, F_T, was then derived from the normal forces per unit arc length, $\Sigma F_N/d\ell$. The canopy cloth stress may be expressed as:

$$F_T = \Delta Pr \tag{31}$$

$$F_T = \frac{\Sigma F_N}{d\ell} \frac{1}{2Cos\phi} \tag{10}$$

$$\Delta Pr = \frac{\Sigma F_N}{d\ell} \frac{1}{2Cos\phi}$$

Substituting equations (3a) and (4) for ΣF_N and solving for the pressure coefficient at any point (X_N, Y_N, β_N) on the load line.

$$CP_N = \frac{\Delta P}{q} = \left(\frac{C_D S_o}{2Cos\beta_o}\right) \frac{sind\beta/2}{rd\ell Cos\phi} \tag{32}$$

Equation (32) illustrates the variables which affect the local pressure coefficient. Another advantage of the load-line approach is that the cloth

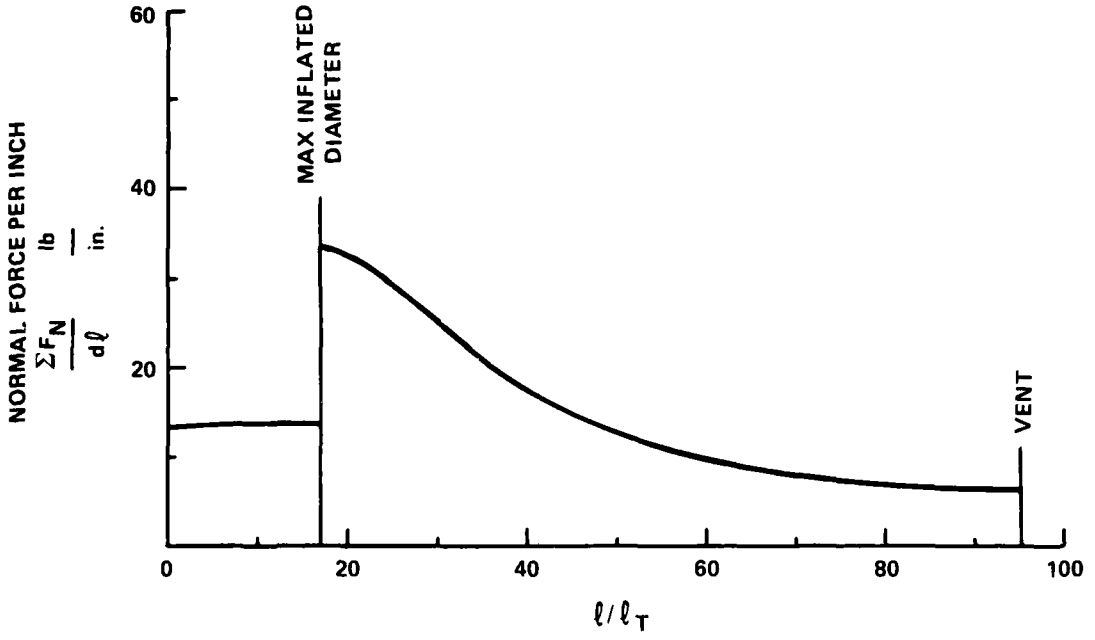

FIGURE 24. NORMAL FORCE PER UNIT OF GORE LENGTH VERSUS PERCENT OF GORE LENGTH FOR THE RINGSLOT PARACHUTE OF EXAMPLE 1

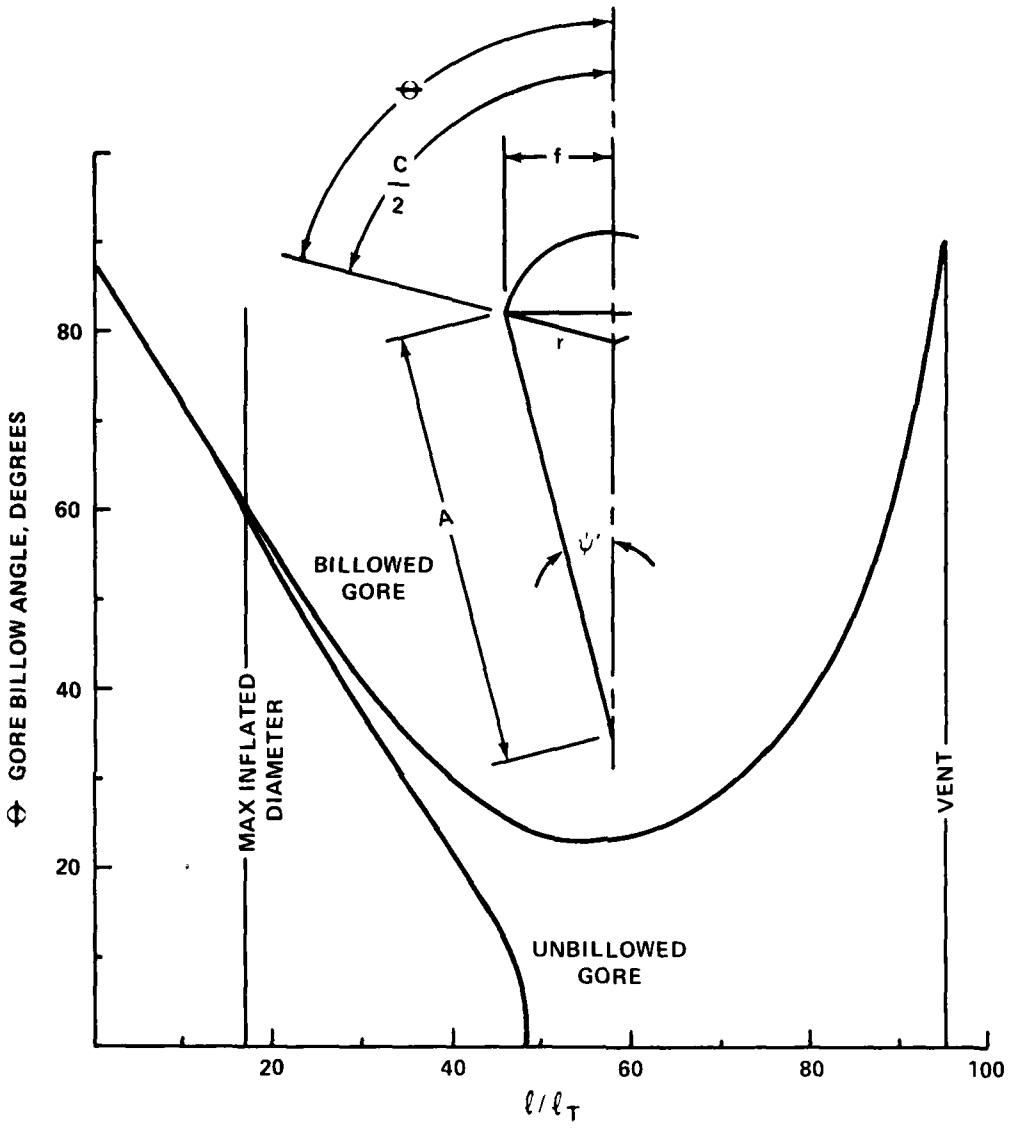

FIGURE 25. EFFECT OF GORE BILLOW ON THE GORE BILLOW ANGLE FOR THE RINGSLOT PARACHUTE OF EXAMPLE 1

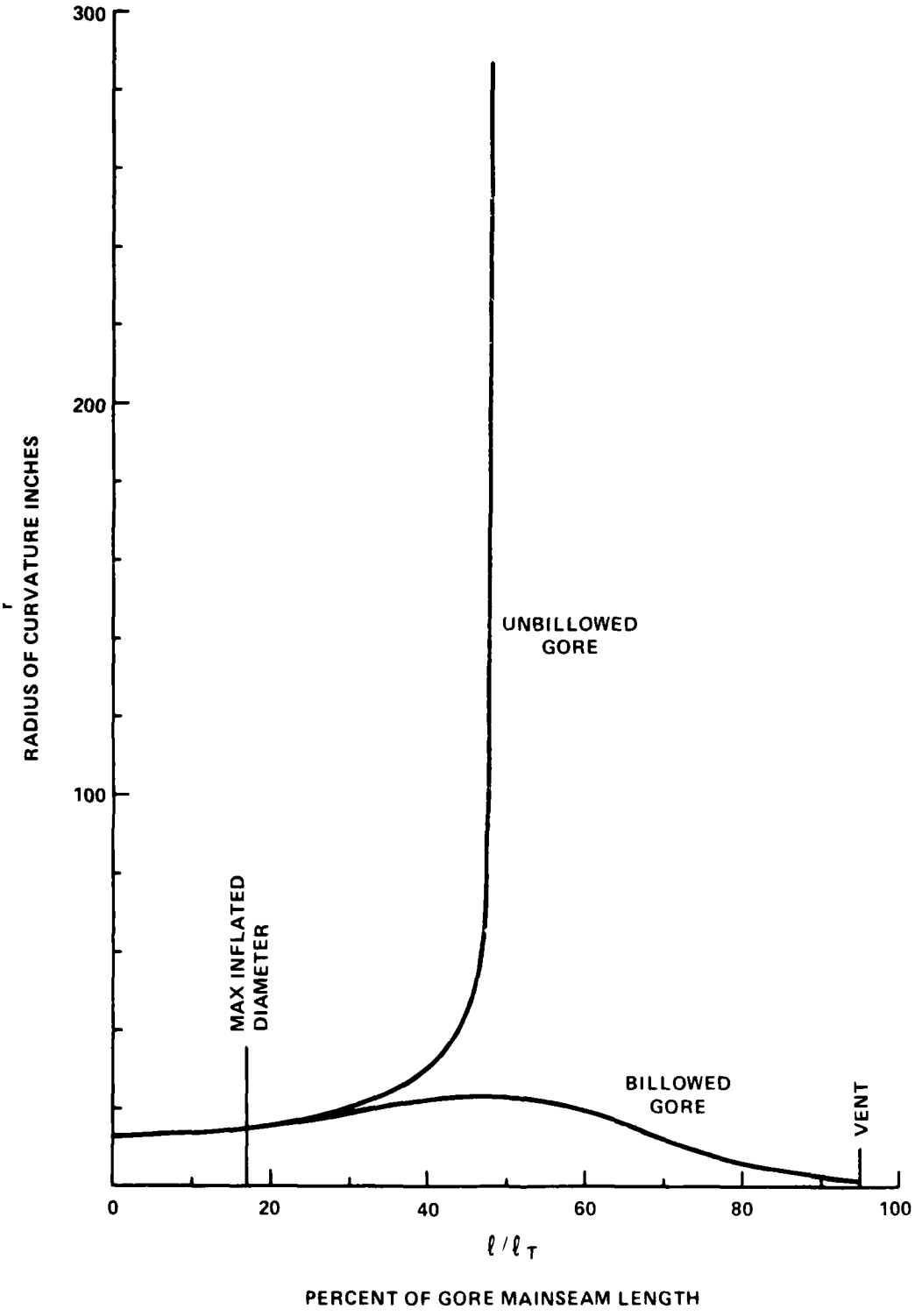

FIGURE 26. EFFECT OF GORE BILLOW ON THE CANOPY CLOTH RADIUS OF CURVATURE FOR THE RINGSLOT PARACHUTE OF EXAMPLE 1

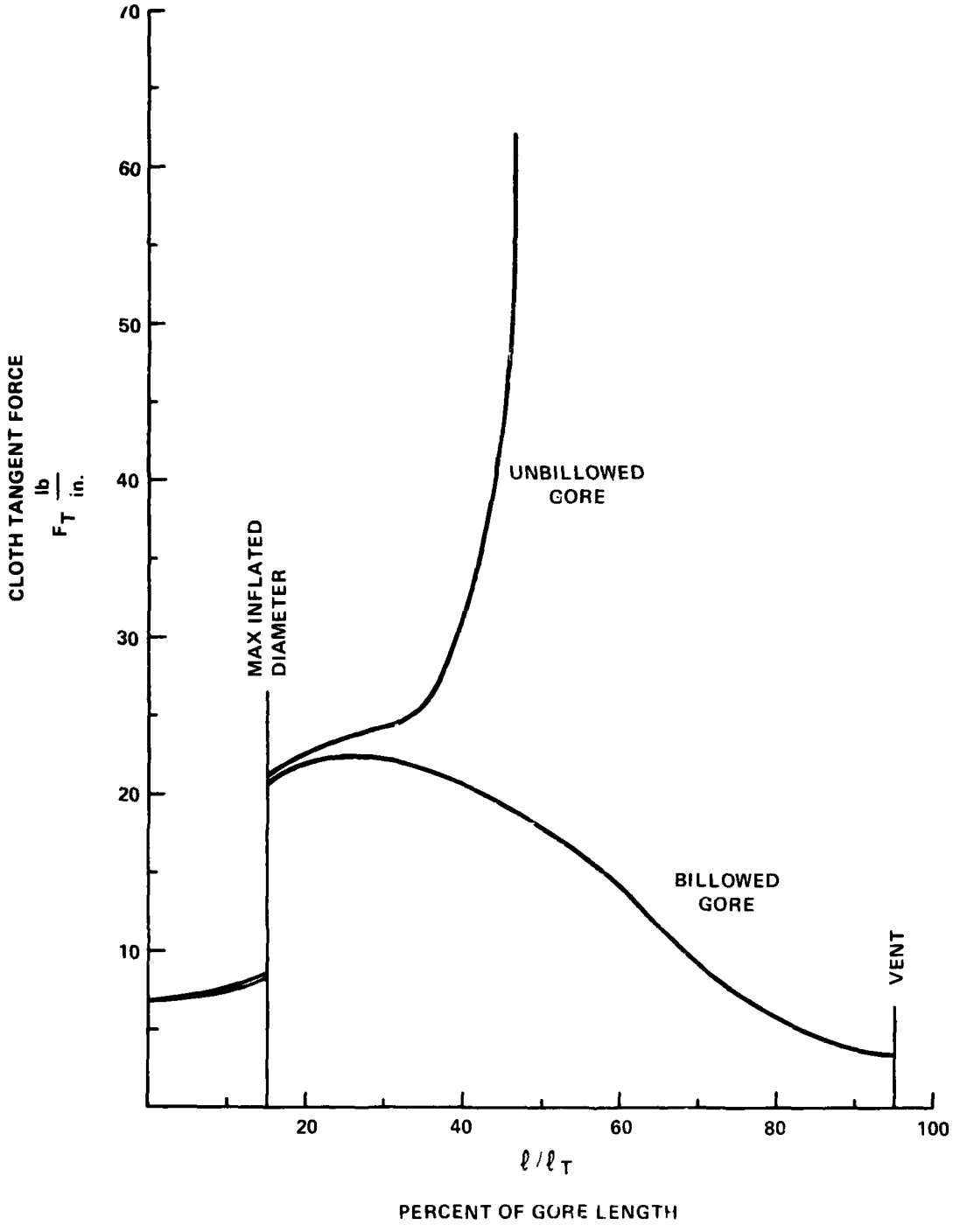

FIGURE 27. CANOPY CLOTH TANGENTIAL FORCE PER UNIT LENGTH VERSUS PERCENT OF GORE LENGTH FOR THE RINGSLOT PARACHUTE OF EXAMPLE 1

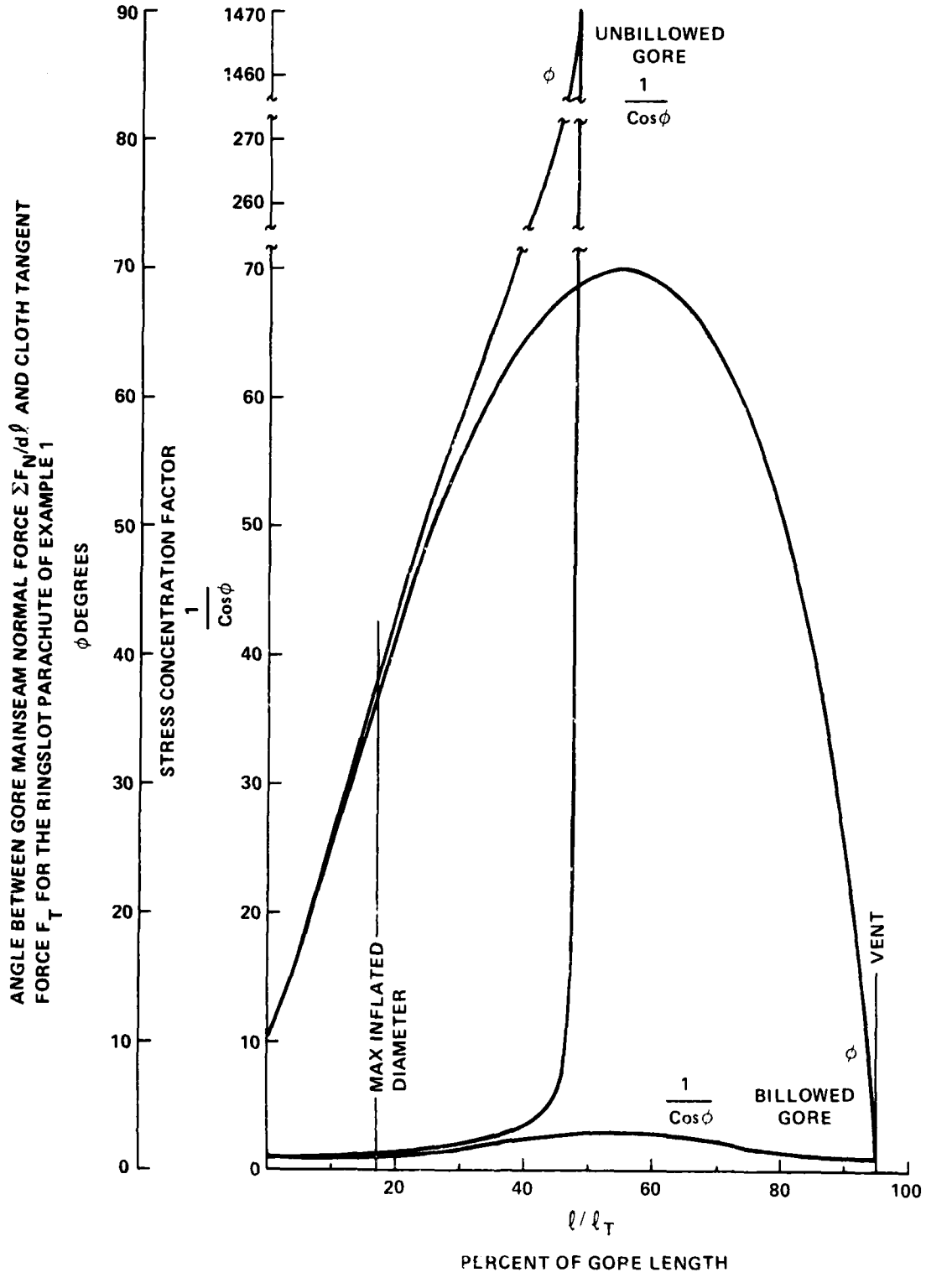

FIGURE 28. EFFECT OF GORE BILLOW ON THE ANGLE ϕ AND STRESS CONCENTRATION FACTOR FOR THE RINGSLOT PARACHUTE OF EXAMPLE 1

tangent force, F_T, and local radius of curvature, r, have been previously independently calculated. Therefore, a more convenient form of pressure coefficient is:

$$F_T = \Delta P r$$

$$\frac{F_T}{qr} = \frac{\Delta P r}{qr} = \frac{\Delta P}{q}$$

$$CP_N = \frac{F_T}{qr} \tag{33}$$

Reference 5 utilizes an average steady state parachute pressure coefficient to calculate the reference inflation time, t_o,* of several types of solid cloth parachutes. The average pressure coefficient was estimated as follows. The parachute steady state drag force may be expressed in two ways:

$$F_D = q\ C_D S_o$$

$$F_D = \Delta P_{av} S_p$$

where S_p is the projected area of the inflated canopy.

$$\Delta P_{av} S_p = q\ C_D S_o$$

$$CP_{av} = \frac{\Delta P_{av}}{q} = \frac{C_D S_o}{S_p}$$

$$S_o = \frac{\pi D_o^2}{4}$$

$$S_p = \frac{\pi D_p^2}{4} \quad \text{(note: } D_p = 2\bar{a}\text{)}$$

*The instant during inflation when the design drag area of the parachute has been achieved for the first time is designated as t_o.

$$K_1 = \frac{D_p}{D_o}$$

$$S_p = \frac{\pi}{4} D_o^2 K_1^2$$

$$\frac{C_D S_o}{S_p} = \frac{C_D(\pi/4)D_o^2}{(\pi/4)\ D_o^2 K_1^2}$$

$$CP_{av} = \frac{C_D S_o}{S_p} = \frac{C_D}{K_1^2} \qquad (34)$$

For a flat circular parachute with a $C_D = 0.75$ and $D_p/D_o = 2/3$.

$$CP_{av} = \frac{0.75}{(2/3)^2}$$

$$CP_{av} = 1.688$$

The average pressure coefficient, CP_{av}, of a fully inflated parachute in steady state is the parachute drag coefficient referenced to the inflated canopy projected area and is subject to variation by all of the parameters that usually alter drag coefficients: i.e., cloth permeability, suspension-line length, etc.

The average pressure coefficient depends upon the canopy drag coefficient and projected diameter. Since these values vary for a given type of parachute, a range of average steady state pressure coefficients is to be expected. Table 2.1 of Reference 4 lists the value range of these parameters for solid textile parachutes. Table 9 lists the expected average pressure coefficient range based on Equation (34) for the data of Reference 4.

The estimated static pressure distribution for the Ringslot Parachute of example 1 is tabulated in Table 6 and graphically illustrated in Figure 29. Figure 29 indicates an apparent radical shift in static pressure distribution between the unbillowed and billowed canopy gores. This is due to the ϕ angle stress concentration factor causing the tangent force in the unbillowed gore to increase at a greater rate than the local radius of curvature.

TABLE 9. RANGE OF AVERAGE STEADY STATE CANOPY PRESSURE COEFFICIENTS

PARACHUTE TYPE	C_D	D_p/D_o	CP_{av}
FLAT	0.75	0.70	1.531
CIRCULAR	0.80	0.67	1.782
EXTENDED	0.78	0.70	1.592
SKIRT	0.87	0.66	1.997
RINGSLOT	0.56	0.67	1.247
	0.65	0.70	1.326
CROSS	0.60	0.72	1.157
	0.78	0.66	1.791

Table 10 is a survey of the effects of gore billow on the canopy pressure distribution. Several values of β_N were selected and the billow at each β_N studied by varying the billowed gore half angle from $\psi = \gamma = 7.5$ degrees to the γ associated with the maximum allowable billow at the canopy vent hem of $\gamma = 7.249$ degrees. For β_N of -60 degrees and -87.5 degrees, γ was limited to 7.45 instead of 7.5. At $\beta_N = -60$ degrees the triangular gore still has stress problems for $\gamma > 7.3$ degrees. At all other β_N angles the pressure coefficients are only slightly affected by billow.

The shift in the theoretical pressure distribution at the maximum inflated diameter is due to the variation of the minor axis length, from b' to b, in the inflated shape. The calculated pressure distribution at the canopy skirt hem is less than one; however, the canopy skirt hem circumferential rings of Ringslot Parachutes have been observed to flutter in field tests indicating a low value of pressure differential.

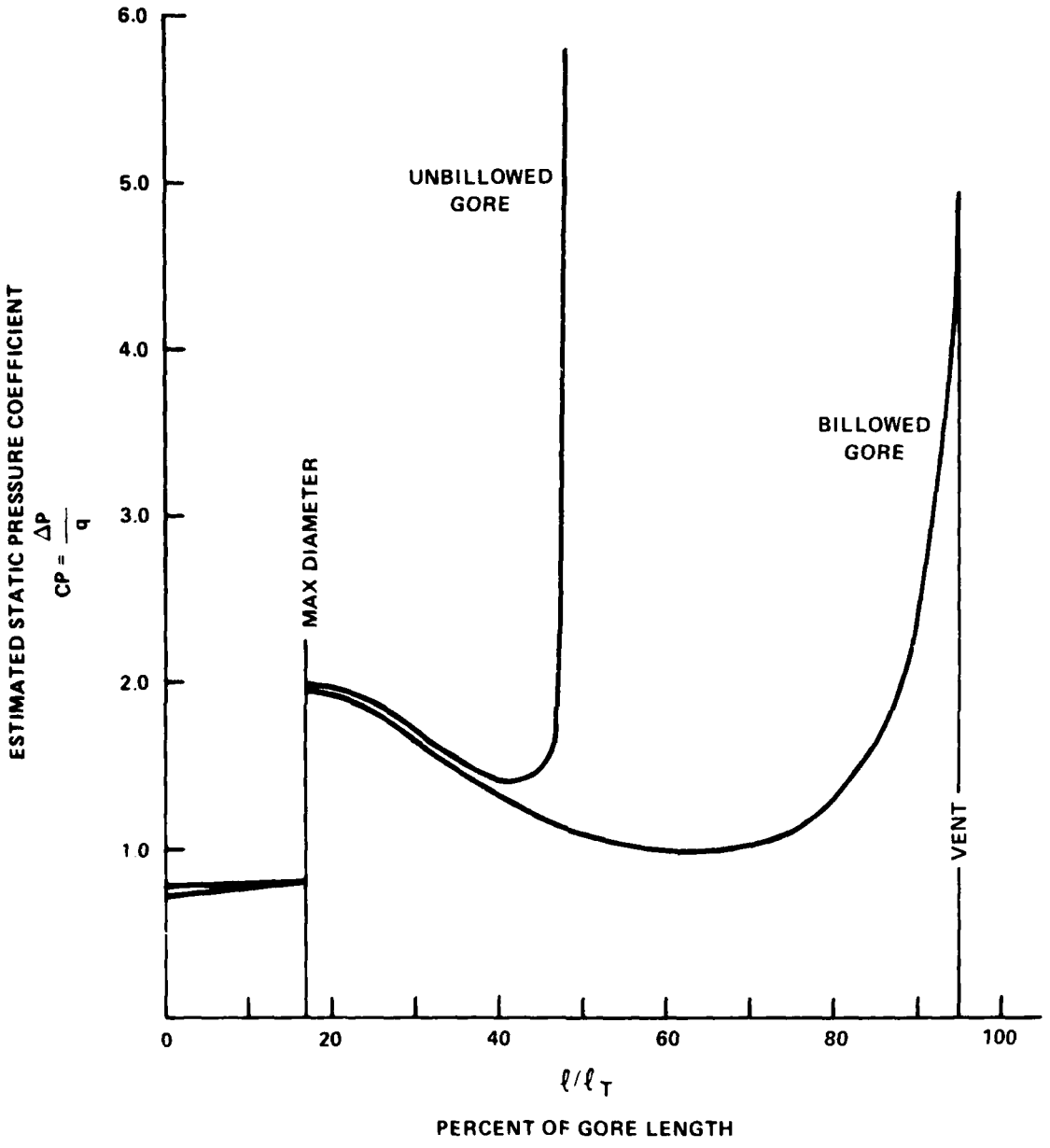

FIGURE 29. ESTIMATED STATIC PRESSURE DISTRIBUTIONS ALONG THE GORE LENGTH FOR BILLOWED AND UNBILLOWED GORES FOR THE RINGSLOT PARACHUTE OF EXAMPLE 1

TABLE 10. EFFECT OF GORE BILLOW ON THE CANOPY PRESSURE DISTRIBUTION

β_N DEG	γ DEG	r_B (IN)	CP
17.9	7.249	12.544	0.732
	7.3	12.544	0.732
	7.4	12.544	0.732
	7.5	12.544	0.732
5	7.249	13.986	0.7830
	7.3	14.005	0.7831
	7.4	14.030	0.7836
	7.5	14.048	0.7840
−0.1	7.249	14.987	1.950
	7.3	15.029	1.951
	7.4	15.082	1.954
	7.5	15.145	1.957
−20	7.249	17.267	1.840
	7.3	17.411	1.844
	7.4	17.659	1.851
	7.5	17.928	1.859
−40	7.249	20.579	1.447
	7.3	21.205	1.458
	7.4	22.512	1.481
	7.5	24.035	1.508
−60	7.249	23.202	1.067
	7.3	26.704	1.101
	7.4	46.883	1.344
	7.45	∞	–
−87.5	7.249	0.979	4.679
	7.3	0.988	4.684
	7.4	1.140	4.696
	7.45	1.578	4.714

REFERENCES

1. Topping, A. D., A Study of Canopy Shapes and Stresses for Parachutes in Steady Descent, WADC TR 55-294, Oct 1955.

2. Ludtke, W. P., A New Approach to the Determination of the Steady-State Inflated Shape and Included Volume of Several Parachute Types, NOLTR 69-159, 11 Sep 1969.

3. Ludtke, W. P., A New Approach to the Determination of the Steady-State Inflated Shape and Included Volume of Several Parachute Types in 24-Gore and 30-Gore Configurations, NOLTR 70-178, 3 Sep 1970.

4. Irvin Industries, Recovery Systems Design Guide, AFFDL TR 78-151, Dec 1978.

5. Ludtke, W. P., "A Technique for the Calculation of the Opening Shock Forces for Several Types of Solid Cloth Parachutes," AIAA Paper 73-477, May 1973.

DEFINITIONS

LOAD LINE

A theoretical replacement of the parachute suspension line and canopy mainseam from the suspension-line confluence point to the canopy vent. The load line has the identical shape of the inflated parachute mainseam.

NORMAL FORCE

The distributed perpendicular force along the load line which provides the inflated canopy shape.

PLANE OF ANALYSIS

The geometric plane, perpendicular to β_N, which contains the gore mainseam coordinates X_N, Y_N, β_N of the surface under analysis and the parachute center line.

TANGENT FORCE

Tensile force in the load line that is tangent to the load line at any arbitrary point.

NOMENCLATURE

A	Perpendicular distance from the tangent at the point X_N, Y_N on the load line to the parachute center line
$\bar{2a}$	Maximum inflated diameter of the gore mainseam
b	Minor axis of the ellipse bounded by the major axis a and the vent of the canopy
b'	Minor axis of the ellipse which includes the canopy skirt hem
C	Circumference of the billowed gore and the width of the gore at the point which is under analysis
C'	Theoretical billowed gore circumference for minimum cloth stress
C_{180}	Theoretical billowed gore circumference for a subtended angle of $2\theta = 180$ degrees
C_D	Parachute drag coefficient
C_DS_O	Parachute steady state drag area, ft^2
CP_N	Pressure coefficient at the point X_N, Y_N, β_N
D_F	Flat constructed canopy diameter
$d\ell$	Incremental length along the load line, inches
d_m	Mouth diameter of the inflated canopy, measured at the junction of the gore mainseam and the canopy skirt hem
D_O	Nominal canopy diameter $= \sqrt{\frac{4S_O}{\pi}}$
D_p	Projected diameter of an inflated parachute
D_R	Design diameter of elliptical and hemispherical shaped gore canopies
F_A	Axial force used to verify the drag force component per suspension line in the load-line force distribution = F_D/Z, lb

NOMENCLATURE (Cont.)

F_{C1}, F_{C2}	Forces in the warp and fill cloth directions in a bias cut canopy, lb/in.
F_{C3}, F_{C4}	Forces in the warp and fill cloth directions in a block cut canopy, lb/in.
F_D	Total parachute drag force, lbs
F_T	A component of the distributed load-line normal force which is tangent to the billowed cloth at the load line - cloth mainseam, lb/in.
ΣF_N	Summation of the normal forces at a point on the load line, lb
F_l	Parachute suspension-line force, lbs; also the tension force tangent to the load line at any arbitrary point
F_N	Summation of the normal forces at a point on the load line, lb
F_{RF}	Stress in the forward hem of a Ringslot Parachute circumferential ring, lb/in.
F_{RR}	Stress in the rear hem of a Ringslot Parachute circumferential ring, lb/in.
F_{tF}	Stress tangent to the gore mainseam at the forward hem of a Ringslot Parachute circumferential ring, lb/in.
F_{tR}	Stress tangent to the gore mainseam at the rear hem of a Ringslot Parachute circumferential ring, lb/in.
2f	Inflated parachute chord line between two adjacent load lines at the point X_N, Y_N, β_N
K_l	Scale factor = $2\bar{a}/D_o$, or D_p/D_o
L	Diameter of the cross-type parachute
L_S	Suspension line length
N	Canopy depth is the distance from the skirt hem of the canopy to the vent of the canopy along the parachute center line
ΔP	Pressure differential between the inside and outside of the parachute canopy at the point X_N, Y_N, β_N, psf
ΔP_{av}	Pressure differential acting on the inflated canopy projected area, psf
q	Dynamic pressure = $1/2\ \rho V^2$, psf
r	Billowed gore radius of curvature

NOMENCLATURE (Cont.)

r'	Billowed gore radius of curvature for minimum stress
S_o	Canopy reference area = $\pi/4\ D_o^2$, ft^2
S_p	Inflated canopy projected area, ft^2
V	Trajectory velocity, fps
W	Width of the arm of a cross-type parachute
X, Y	Coordinates in the plane of analysis is that contains the load line
X_N, Y_N	Coordinates of the point under analysis where the normal force is considered to be acting
Z	Number of gores in the parachute
α_F	Rake angle on the leading hem edge of a Ringslot Parachute circumferential ring, degrees
α_R	Rake angle on the trailing hem edge of a Ringslot Parachute circumferential ring, degrees
ß	Slope angle at the point X, Y between the load line and the parachute center line, degrees
$ß_N$	Slope angle at the point X_N, Y_N between the load line and the parachute center line, degrees
$ß_o$	Semi-vertex angle between the suspension lines and the parachute center line, and tangent angle of the mainseam canopy hem, degrees
dß	A small change in angle ß, degrees
γ	Semi vertex angle of the billowed parachute gore, degrees
θ	Central angle subtended by the billowed gore, degrees
θ'	Central angle subtended by the billowed gore for minimum stress, degrees
μ	Smaller acute angle between the tapered gore edge and the direction of the fiber in a bias cut gore, degrees
ρ	Air density, slugs per ft^3
τ	Angle between the billowed gore radius of curvature and the length A, degrees
ϕ	Angle between the load line normal force and the force tangent to the canopy cloth at the load line, degrees

NOMENCLATURE (Cont.)

2ψ	Angle subtended by a parachute gore in the plane of the canopy mouth = 360°/Z; also the unbillowed gore vertex angle, degrees
$2\psi'$	Angle subtended by a parachute gore in the plane perpendicular to the load line at the point X_N, Y_N, β_N, degrees

DISTRIBUTION

	Copies
Commander Naval Air Systems Command Attn: Library Washington, DC 20361	5
Commander Naval Sea Systems Command Attn: Library Washington, DC 20362	5
Commanding Officer Naval Ship Research and Development Center Attn: Library Washington, DC 20007	2
Office of Naval Research Attn: Library Washington, DC 20360	4
U. S. Naval Academy Attn: Library Annapolis, MD 21402	2
Commanding Officer U. S. Naval Air Development Center Attn: Library Thomas J. Popp Maria C. Hura Johnsville, PA 18974	2 1 1
Commanding Officer U. S. Army Mobility Equipment Research and Development Center Attn: Technical Document Center Fort Belvoir, VA 22660	2
Commander U. S. Army Aviation Systems Command Attn: Library St. Louis, MO 63166	2
Commander U. S. Army Munitions Command Attn: Technical Library Dover, NJ 07801	2
Commander U. S. Army Weapons Command Attn: Technical Library Research and Development Directorate Rock Island, IL 61201	2
Commander U. S. Army ARRADCOM Attn: Library Thomas D. Hoffman DRDAR-LCA-F Ray W. Kline DRDAR-LCA-F Dover, NJ 07801	1 1 1
Commander U. S. Army Natick R&D Labs Attn: Library Calvin K. Lee M. P. Gionfriddo Joseph Gardella Timothy E. Dowling DRDNA-UAS Kansis Street Natick, MA	2 1 1 1 1

DISTRIBUTION (Cont.)

	Copies
Commanding Officer	
Wright Patterson AFB	
Attn: William Casey ASD/ENECA	1
William Pinnell AFWAL/FIER	1
Robert L. Hesters Jr. ASD/YYEE	1
E. Schultz AFWAL/FIER	1
Daniel J. Kolega Bldg. 25 Area B	1
Patrick J. O'Brian Bldg. 25 Area B	1
H. Engel ASD/ENEC	1
OH 45433	
Commanding Officer	
Air Force Flight Test Center	
Attn: Airframe Systems Division Aerodynamics Decelerator Branch	2
Edwards AFB	
CA 93523	
Commanding Officer	
Air Force Space Division	
Attn: Library	2
P. O. Box 92960	
Worldway Postal Center	
Los Angeles, CA 90009	
Commanding Officer	
Air Force Aerophysics Laboratory	
Attn: Library	2
Hanscom Field, MA	
Commanding Officer	
Kelly AFB	
Attn: SA-ALC/MMIR	2
Library	2
TX 78241	
Commanding Officer	
McCallan AFB	
Attn: Library	2
SA-ALC/MMIR	2
CA 95652	
Defense Technical Information Center	
Cameron Station	
Alexandria, VA 22314	12

	Copies
Library of Congress	
Attn: Gift and Exchange Division	
Washington, DC 20540	
NASA Langley Research Center	
Langley Station	
Attn: Research Program Recording Unit, Mail Stop 122	1
Raymond L. Zavasky, Mail Stop 177	1
Andrew S. Wright, Jr., Mail Stop 401	8
Hampton, VA 23365	
NASA Ames Research Center	
Attn: Library, Stop 202-3	1
Moffett Field, CA 94035	
NASA Flight Research Center	
Attn: Library	1
P. O. Box 273	
Edwards, CA 93523	
NASA Goddard Space Flight Center	
Attn: Library	1
Greenbelt, MD 20771	
Jet Propulsion Laboratory	
4800 Oak Grove Drive	
Attn: Library, Mail 111-113	1
Pasadena, CA 91103	
NASA Manned Spacecraft Center	
Attn: Library, Code BM6	1
2101 Webster Seabrook Road	
Houston, TX 77058	
NASA Marshall Space Flight Center	
Attn: Library	1
Huntsville, AL 25812	
NASA Goddard Space Flight Center/ Wallops Flight Facility	
Attn: Library	1
Mr. Mendle Silbert	1
Mr. Anel Flores	1
Wallops Island, VA 23337	

DISTRIBUTION (Cont.)

	Copies
NASA Lewis Research Center Attn: Library, Mail Stop 60-3 21000 Brookpark Road Cleveland, OH 44135	1
NASA John F. Kennedy Space Center Attn: Library, Code IS-CAS-42B Kennedy Space Center, FL 32899	1
NASA Headquarters Attn: Library Washington, DC 20546	2
Sandia National Laboratories Attn: Code 1632	1
Library	1
Dr. Dean Wolf	1
Dr. Carl Peterson	10
R. Kurt Baca	1
Albuquerque, NM 87185	

	Copies
University of Minnesota Dept. of Aerospace Engineering Attn: Dr. W. L. Garrard Minneapolis, MN 55455	2
Internal Distribution:	
U13 (W. P. Ludtke)	75
U13 (J. F. McNelia)	1
U13 (D. W. Fiske)	1
U13 (J. Murphy)	1
U13 (J. G. Velez)	1
U13 (R. Tarulli)	1
U13 (A. G. Fritz)	1
U13 (R. L. Pense)	1
U13 (C. J. Diehlman)	1
U131 (E. Noel)	1
U43 (J. Rosenberg)	1
U43 (B. Delre)	1
E431	9
E432	3

END

FILMED

1-85

DTIC